AGU ADVANCING EARTH AND SPACE SCIENCES

Water Resources Research

RESEARCH ARTICLE
10.1029/2024WR037268

A Scale-Adaptive Urban Hydrologic Framework: Incorporating Network-Level Storm Drainage Pipes Representation

Taher Chegini[1], Hong-Yi Li[1], Y. C. Ethan Yang[2], Günter Blöschl[3], and L. Ruby Leung[4]

[1]Department of Civil and Environmental Engineering, University of Houston, Houston, TX, USA, [2]Department of Civil and Environmental Engineering, Lehigh University, Bethlehem, PA, USA, [3]Institute of Hydraulic Engineering and Water Resources Management, Vienna University of Technology, Vienna, Austria, [4]Atmospheric, Climate & Earth Sciences Division, Pacific Northwest National Laboratory, Richland, WA, USA

Key Points:

- Network-level representation of stormwater pipes balances physical basis, parameter parsimony, and computational efficiency
- Scale-adaptive parameterization using Graph Theory enables modeling across diverse urban watersheds
- Nonlinear, threshold relationship is revealed between stormwater pipe network characteristics and flood reduction in urban watersheds

Correspondence to:

H.-Y. Li,
hongyili.jadison@gmail.com

Citation:

Chegini, T., Li, H.-Y., Yang, Y. C. E., Blöschl, G., & Leung, L. R. (2025). A scale-adaptive urban hydrologic framework: Incorporating network-level storm drainage pipes representation. *Water Resources Research*, *61*, e2024WR037268. https://doi.org/10.1029/2024WR037268

Received 1 FEB 2024
Accepted 20 JAN 2025

Author Contributions:

Conceptualization: Taher Chegini, Hong-Yi Li
Data curation: Taher Chegini
Formal analysis: Taher Chegini, Hong-Yi Li
Funding acquisition: Hong-Yi Li
Investigation: Taher Chegini, Y. C. Ethan Yang, Günter Blöschl, L. Ruby Leung
Methodology: Taher Chegini, Hong-Yi Li
Project administration: Hong-Yi Li
Resources: Hong-Yi Li
Software: Taher Chegini
Supervision: Hong-Yi Li
Validation: Taher Chegini
Visualization: Taher Chegini
Writing – original draft: Taher Chegini
Writing – review & editing: Hong-Yi Li, Y. C. Ethan Yang, Günter Blöschl, L. Ruby Leung

Abstract Below-ground urban stormwater networks (BUSNs) significantly influence urban flood dynamics, yet their representation at the watershed or larger scales remains challenging. We introduce a scalable urban hydrologic framework that centers on a novel network-level BUSN representation, balancing the needs for physical basis, parameter parsimony, and computational efficiency. Our framework conceptualizes an urban watershed into four interacting zones: hillslopes (natural), storm-sewersheds (urban), a sub-network channel (tributaries), and a main channel. We develop an innovative Graph Theory-based algorithm to derive network-level BUSN parameters from publicly available datasets, enabling efficient, scalable parameterization. We demonstrate this framework's applicability at nine representative watersheds in the Houston metropolitan region, USA, with urban imperviousness ranging from 0% to 64% and drainage areas ranging from 24 to 302 km^2. Our model achieves satisfying computational efficiency, completing hourly time step simulations for 18 years in less than 5 sec per watershed on a standard PC. Validation against observed daily streamflow confirms that the model can capture small-to-large flood peaks and seasonal and annual water balance over these watersheds. Comparisons with the National Water Model show better performance in predicting flood peaks and overall water balance, underscoring the promises of our new framework for urban hydrologic modeling at large scales. Furthermore, analysis reveals nonlinear relationships between BUSNs' designed capacities and flood reduction effects. Our approach bridges the gap between detailed hydraulic and large-scale hydrologic models, providing a valuable tool for urban flood prediction and management across broader spatial and temporal scales.

Plain Language Summary Cities often flood during heavy rains, with underground pipes playing a big role. However, including these pipes in flood predictions for large areas is challenging due to a lack of data and computational demands. We created a new way to model city flooding that simplifies the underground pipe system while maintaining accuracy. Our method divides a city into four parts: natural areas, areas draining into pipes, smaller streams, and main rivers. We developed an algorithm to generate pipe networks using freely available information. Testing our model in nine areas around Houston, Texas, with varying urban development, we found it can predict 18 years of flooding in seconds on a regular computer. Our predictions matched well with actual flood data for both big and small floods, outperforming a well-known national flood model. Our results also show that adding more pipes doesn't always reduce flooding as much as expected. This new method could help cities better predict and manage flooding over large areas and long time periods, addressing a critical gap in urban flood modeling.

1. Introduction

Rapid global urbanization and accelerating climate change fundamentally modify hydrologic processes by altering hydrologic conditions (e.g., imperviousness, soil compaction) and intensifying extreme climate events. Moreover, urbanization and climate change exhibit complex interplay, potentially amplifying their individual effects (Garschagen & Romero-Lankao, 2015; Grimm et al., 2008). These changes significantly impact urban hydrologic cycles and often lead to increased storm runoff and flood risks (Miller & Hutchins, 2017; Yang et al., 2013). Below-ground urban stormwater networks (BUSNs) are essential for mitigating urban floods, underscoring why their modification—primarily through upgrades or duplication, such as replacing pipes with larger ones—remains a predominant, albeit costly and disruptive, flood mitigation strategy (Argue &

Pezzaniti, 2012; Burns et al., 2015; Chocat et al., 2001). Historically, the impacts of urbanization and climate change often manifest themselves and are usually studied at the large spatial (regional and larger) and long temporal (decadal and longer) scales (Miller & Hutchins, 2017; Yang et al., 2013). Therefore, there is a critical need for a predictive understanding of urban hydrologic processes at large spatial and long temporal scales that can quantitatively account for the effects of urban infrastructures and landscape properties under urbanization and climate change.

However, current models struggle to capture both large-scale, long-term trends and localized, short-term hydrologic events, particularly in urban environments (Cristiano et al., 2017; Hutchins et al., 2017; Salvadore et al., 2015). Existing models involving urban hydrologic processes are concentrated at two ends of a spectrum: hydrologic models that can run at large spatial and long temporal scales, and hydraulic-based models that describe fine-scale urban processes in detail and typically run at the local scale and over relatively short periods. However, both have their limitations, necessitating the need for a strategy to fill this gap. Most current large-scale models focus on surface urban processes. Examples of such models are the National Water Model (NWM) developed by the National Oceanic and Atmospheric Administration of the US (Cosgrove et al., 2024), the Energy Exascale Earth System Model sponsored by the US Department of Energy (E3SM Project, 2024), and the Global Flood Awareness System developed by the Joint Research Centre of the European Commission (Harrigan et al., 2020). These models, despite being indispensable for understanding regional and global water cycles under climate change, operate at resolutions too coarse to capture fine-scale heterogeneity in urban environments, for example, completely missing BUSNs and their interactions with urban surface hydrologic processes. This oversimplification, although historically owing to data scarcity, leads to inaccuracies in predicting urban floods and other urban hydrologic processes such as infiltration, evapotranspiration, groundwater recharge, etc.

Hydraulics-based models, such as the Storm Water Management Model (SWMM) (Avellaneda et al., 2017; W. Chen et al., 2022; McGrath et al., 2019; Morales et al., 2016; Rossman & Simon, 2022; Sytsma et al., 2022;) and MIKE-URBAN (DHI, 2023), are invaluable for detailed urban hydraulic and hydrologic simulations. The integration of storm sewer networks into hydrologic-hydraulic models is essential for accurately representing urban flood dynamics, as these networks play a pivotal role in managing stormwater runoff and mitigating flood risks (Dong et al., 2022; Guo et al., 2021; Vemula et al., 2018; Wong & Kerkez, 2018). In these models, for example, BUSNs are represented at the level of individual stormwater pipes, with water and other fluxes simulated using hydraulic equations. These models nonetheless have their own limitations, such as intensive data requirements, expensive computational costs, and site-specific parameters not easily transferable (Fraga et al., 2016; Freni et al., 2009; Meyers et al., 2021; Nanía et al., 2015; Naves et al., 2019). Consequently, these limitations constrain the usage of hydraulics-based models to typically small scales and limited places where data quantity and quality requirements are met, making them impractical for large-scale, long-term urban hydrologic modeling.

To address this knowledge gap between the two categories of models, we propose a new modeling strategy that represents BUSNs directly at the network level, capturing their main hydrologic functions (e.g., taking urban excess runoff, temporarily storing it before discharging to water bodies, hence ultimately mitigating urban floods) instead of modeling individual pipes and their interactions. Correspondingly, our BUSN parameterization centers on a new algorithm based on Graph Theory to delineate storm-sewersheds within a watershed, derive sub-BUSNs associated with each storm-sewershed, and determine the BUSN-relevant parameters a priori. We implement such a modeling strategy in the form of a new urban hydrologic model that is physically based, parameter-parsimonious, and computationally efficient, holding promises to be applied at large spatial and long temporal scales without losing sight of below-ground urban hydrologic processes.

As a proof of concept, we demonstrate this modeling framework to nine representative watersheds exhibiting various levels of urbanization, ranging from natural to highly developed watersheds in the Houston metropolitan area, Texas, US. This region is chosen for its diverse landscape and rich history of floods. This demonstration allows us to evaluate the model's performance across a spectrum of urban environments and prove its adaptability and promises for broader applications. We also compare our model's performance against the National Water Model (NWM) version 3, demonstrating the importance of incorporating BUSNs in watershed-scale urban hydrological modeling and highlighting the potential improvements our approach offers.

In the following sections, we detail our modeling framework (Section 2), explain the input data preparation and parameterization strategy (Section 3), and evaluate the model's performance across nine representative

10.1029/2024WR037268

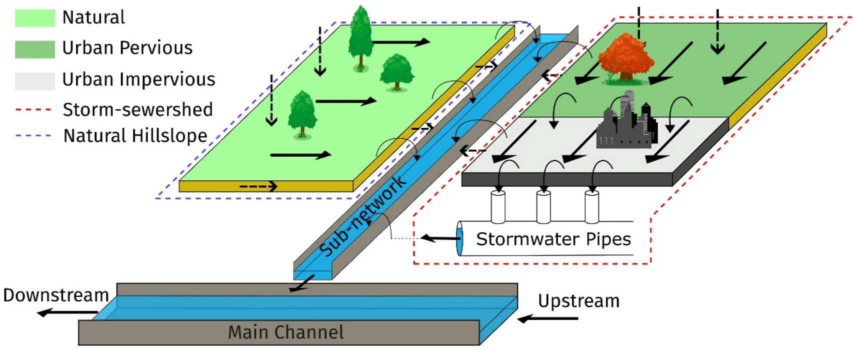

Figure 1. Conceptual diagram of the proposed modeling framework.

watersheds in the Houston metropolitan area, Texas, US (Section 4). Section 5 examines the parameter sensitivity. Section 6 discusses in-depth the impacts of BUSNs on urban flooding. Section 7 synthesizes our major findings and implications and lists out limitations and future directions. Section 8 concludes with a summary.

2. Modeling Framework

Here we introduce our overall modeling framework, including the conceptualization, governing equations, and numerical methods. This framework is generalizable and applicable to any urban watershed.

2.1. Conceptualization

A natural watershed can be conceptualized into three components with distinct hydrologic functions and hydrologically connected to each other (Li et al., 2013): (a) Hillslopes, where the natural landscape and soil conditions control runoff generation and routing processes, (b) a sub-network channel, which receives runoff from hillslopes and discharges the runoff into a single main channel, and (c) the main channel, which receives the discharge from sub-network and connects the local watershed with its upstream and/or downstream watersheds. Following Li et al. (2013), we do not explicitly represent each tributary within a watershed but conceptualize all the tributaries into a hypothetical, single sub-network channel with a transport capacity equivalent to all the tributaries combined. If a watershed is sufficiently small, only one river segment is within it. In such a case, there will be no sub-network channel but only a main channel.

For urban watersheds, we extend such conceptualization by adding a fourth component, storm-sewersheds, where urban runoff generation and routing processes are governed by man-made infrastructure such as BUSNs and impervious areas, as shown in Figure 1. We define a storm-sewershed as an urban area (typically a mixture of both pervious and impervious surfaces) and its corresponding BUSN that contributes stormwater to rivers and other surface waterbodies via a single outfall (Hung et al., 2020). Such a network-level representation of stormwater pipes avoids detailed hydraulic modeling of individual pipes and their interactions. Yet it captures major hydrologic functions of BUSNs at the watershed scale, including (a) interception capacity, that is, the maximum amount of surface runoff from impervious areas that can be captured and passed into stormwater pipes via street inlets and catch basins (Chegini & Li, 2022); (b) conveyance capacity, that is, the maximum discharge that can be routed through BUSN pipes into receiving water bodies via outfalls; and (c) transient storage capacity, that is, the total amount of water that can be stored in all the BUSN pipes during a storm event.

BUSNs are designed to rapidly direct stormwater to the nearest waterbodies, minimizing potential flooding impacts (Brown et al., 2009). Considering that outfalls are the only locations where a BUSN discharges stormwater back to surface water and the fact that these outfalls are distributed over urban areas, it is neither necessary nor feasible for all pipes within a BUSN to be well-connected. Furthermore, the pipes within a BUSN that are well-connected form a cluster in which their required drainage capacities are not necessarily equal. For example, a residential area's required stormwater drainage capacity differs from that of a business or industrial area. For convenience, we denote such a cluster of stormwater pipes as a sub-BUSN. We then define a storm-sewershed based on a sub-BUSN. Within a storm-sewershed, stormwater pipes are well-connected, and all contribute to a single outfall that discharges into a surface waterbody, but they are not connected to the other sub-

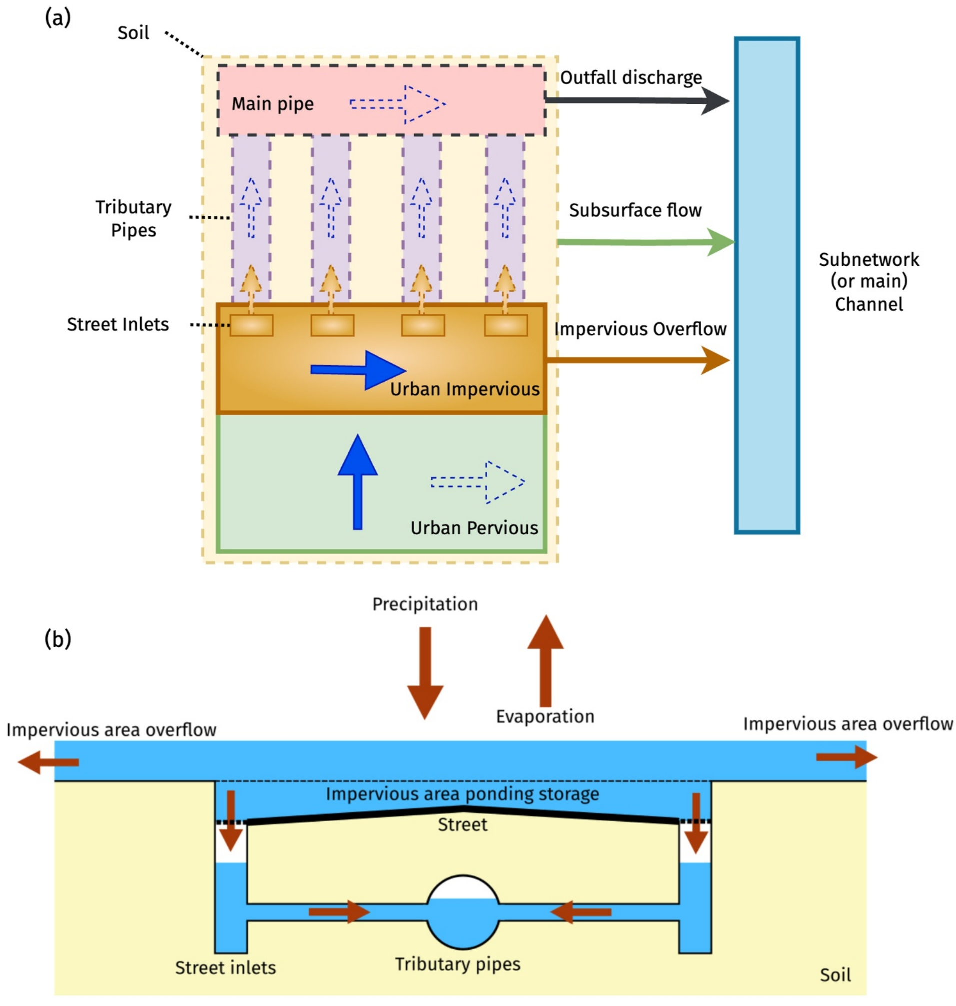

Figure 2. Diagram of a storm-sewershed: (a) A plan view of major elements and their flow exchanges; (b) a cross-section view of urban impervious surface, street inlets, stormwater pipes, and their connections.

BUSNs even in the same watershed. We can thus discretize the urban portion of a watershed into several storm-sewersheds (using the techniques based on Graph Theory; more details are provided later in Section 3.1.2).

As shown in Figure 2, a storm-sewershed consists of both surface and subsurface elements that collectively determine the urban hydrologic responses to storms, including urban pervious surfaces (e.g., lawns, parks), impervious surfaces (such as streets, buildings, and parking lots), a sub-BUSN, an outfall connecting the sub-BUSN to the sub-network channel (or the main channel if there is no sub-network channel), and soils surrounding the stormwater pipes within the sub-BUSN. For simplicity, we lump all urban pervious surfaces into a single pervious surface zone. Similarly, we define a lumped impervious surface zone. Considering that most streets can store some surface runoff temporarily before discharging into the sub-BUSN via inlets, we also assume there is a limited storage capacity in the urban impervious surface zone. Within each sub-BUSN, there are several stormwater pipes. We denote the pipe directly connected to the outfall as the main pipe and the rest as the tributary pipes. These tributary pipes function as the connection between street inlets and the main pipe. Thus, we replace all tributary pipes that connect an inlet to the main pipe with a single equivalent pipe. As a result, in our simplified sub-BUSN, there is a one-to-one match between a street inlet and a tributary pipe, that is, the number of tributary pipes is the same as the number of street inlets.

Overall, when rain falls on an urban watershed, any surface runoff generated from the urban pervious surface zone will route into the impervious surface zone and join the surface runoff generated there. The ponding water on the impervious surface zone may evaporate into the atmosphere, enter into the sub-BUSN zone via street inlets

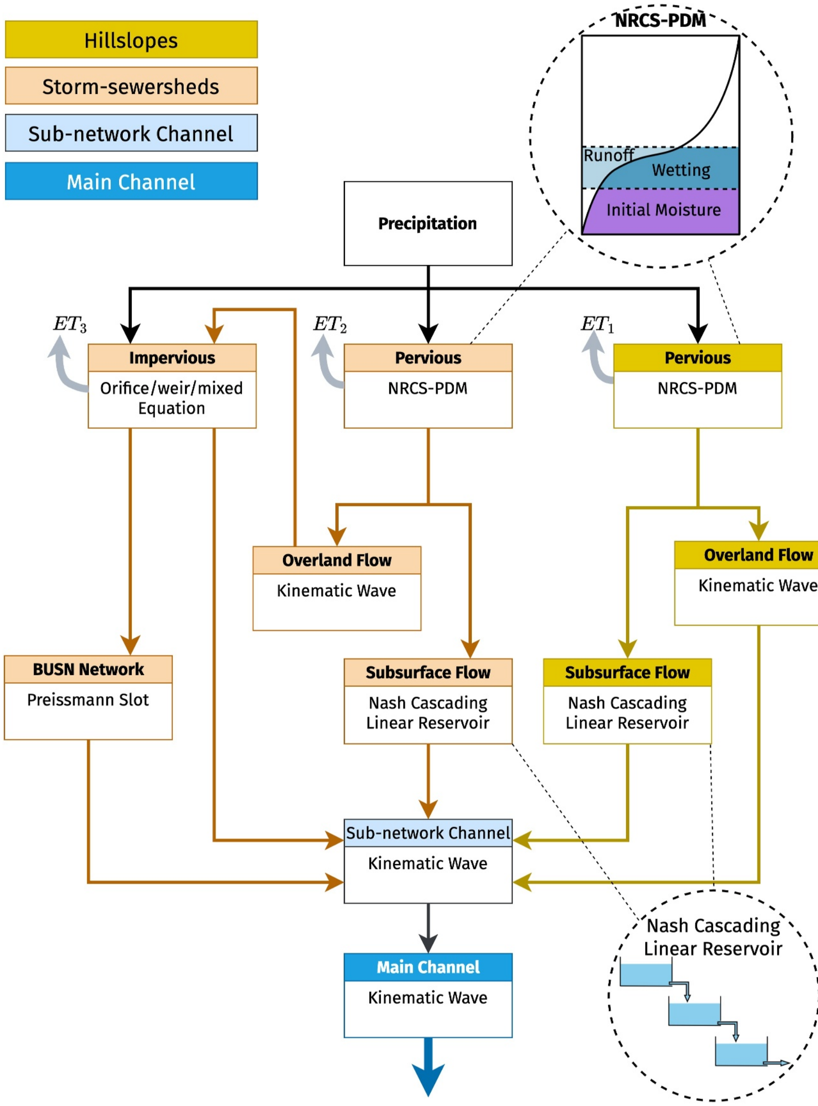

Figure 3. Flowchart of the proposed modeling framework.

distributed along streets, or overflow across the surface zones into the sub-network or main channel when the amount of water stored in the impervious surface zone exceeds its storage capacity (i.e., urban flooding occurs). Tributary pipes receive stormwater via street inlets and discharge to the main pipe. The main pipe discharges into the sub-network channel via the outfall. More detailed process descriptions are provided next in Section 2.2. Note that there are two major types of urban sewer systems: separate sewer systems, where two separate pipe systems carry stormwater and sanitary sewage, respectively, and combined sewer systems, where a single pipe system exists for conveying both stormwater and municipal sewage. In this study, we only deal with stormwater and leave out sanitary sewage for future work.

2.2. Governing Equations and Numerical Methods

This section describes major hydrologic processes included in the model, the corresponding governing equations, and the numerical method, as shown in Figure 3.

2.2.1. Hillslope Processes

Hillslope processes include runoff generation and routing across natural areas. Runoff generation processes are simulated using a recently developed runoff scheme that unifies the Natural Resources Conservation Service

(NRCS, formerly known as the Soil Conservation Service) Curve Number (CN) method (SCS, 1972) and the Probability Distribution Model (PDM) (Moore & Clarke, 1981), denoted as NRCS-PDM hereinafter (Wang, 2018; Yao et al., 2020a). The NRCS-CN method is a runoff scheme originally derived from empirical data analysis at the small watershed scale over the U.S (SCS, 1972). It has been extensively applied in the U.S. for simulating surface runoff over natural and urban areas in the U.S. and other countries (Krajewski et al., 2020; Mishra et al., 2012; Shrestha et al., 2021). The NRCS-PDM scheme offers a theoretical interpretation of the NRCS-CN method in terms of probabilistic distributions of soil water storage capacity (Wang, 2018), and is more suitable for simulating surface and subsurface runoff across event, daily, and monthly time steps (Yao et al., 2020a). In NRCS-PDM, there are three parameters controlling runoff generation: Soil storage capacity (Sb_n), shape factor (a), and surface/subsurface runoff partitioning coefficient (γ), which we use in this study.

The routing of surface and subsurface runoff in NRCS-PDM is controlled by two other parameters subject to calibration (Yao et al., 2020a). In this study, surface runoff is routed across hillslopes as overland flow using Manning's equation (for kinematic wave routing) (Chow et al., 1988):

$$Q = \frac{\sqrt{S_0}}{n} R_h^{2/3} A, \tag{1}$$

where Q is discharge (m^3/s), S_0 is routing surface slope (m m^{-1}), n is Manning's roughness coefficient, R_h is hydraulic radius (m), and A is cross-sectional area (m^2). Note that Manning's equation is a hydrologic routing method that is a simplified description of the full Saint-Venant equation (aka, hydraulic equation), hence computationally inexpensive. It applies to both overland flow and channel routing (Chow et al., 1988). Subsurface flow is routed using the Nash cascading reservoir method (Nash, 1957) with three serial linear reservoirs. The discharge rate from each reservoir is estimated as:

$$Q_r = S_r k_b, \tag{2}$$

where Q_r is discharge (m^3/s), S_r is reservoir storage (m^3), and k_b is residence time (s^{-1}). For simplicity, we assume all three reservoirs have the same residence time, that is, the same k_b value.

2.2.2. Storm-Sewershed Processes

Storm-sewershed processes include runoff generation and routing across urban areas. In the urban pervious portion of each storm-sewershed, surface and subsurface runoff generation and evaporation processes are also simulated using the NRCS-PDM scheme. The only difference is that we adjust the soil storage capacity of the urban pervious part to reflect soil compaction (more details are provided later in Section 3). Similarly, overland and subsurface flow in the urban pervious portion are simulated using Manning's equation and the Nash cascading linear reservoir method, respectively.

In the impervious portion, we estimate evaporation as the minimum between potential evapotranspiration (PET) and surface ponding water depth. The flow rate of surface ponding water entering the sub-BUSN via an inlet is estimated using the Urban Drainage and Flood Control District model (UDFCD-CSU) (UDFC, 2016). This model assumes that the discharge through an inlet may occur under one of the three conditions: weir flows when ponding water depths above the inlets are shallow, orifice flows when ponding water depths are deep, or mixed flows when ponding water depths are intermediate. Instead of pre-determining the exact condition, the model calculates all three flow rates and takes the minimum of these three as the inlet's interception capacity. Urban flooding may occur at any time if the amount of surface water stored in the impervious surface zone exceeds its storage capacity. As such, the overflow from the impervious surface zone is routed directly into the sub-network channel using Manning's equation.

Flow through the tributary and main pipes is also simulated using Manning's equation, assuming circular cross-sections for both the tributary and main pipes. In contrast to open channel flow, pipe flow can become pressurized when a pipe is full. In such a case, Manning's equation is not directly applicable, since it is for open channel flows. Thus, we adopt the Preissmann Slot method (Cunge & Wegner, 1964) to enforce some special treatment of the cross-section geometry of pressurized pipes. Such treatment allows the pipes to be numerically simulated as open channels using Manning's equation. Briefly, this method artificially adds a narrow slot on a pipe's crown, transforming pipe pressurized flow conditions to those of open channel flow, and thus allows us to invoke the kinematic wave assumption. These storm-sewershed processes are parallel to but do not interact with those hillslope processes. They interact with the sub-network channel by discharging runoff into it.

2.2.3. Sub-Network and Main Channel Processes

Routing through the sub-network and main channels is simulated using Manning's equation. Similar to Li et al. (2013), we assume the cross-section geometry of the sub-network channel is rectangular. For a main channel, we assume the cross-section geometry is rectangular (with a bankfull width and depth) when the channel water depth is not higher than the corresponding bankfull depth. Once the channel water depth exceeds the bankfull depth, the cross-section will first become trapezoidal and then rectangular again, with a wider width equal to an adjustment coefficient multiplying the bankfull width. The adjustment coefficient should be larger than 1.0 to mimic the effects of floodplains. In this study, it is set as 3.0 for urban watersheds after some trials instead of 5.0 as in Li et al. (2013), since the floodplains of urban rivers are typically narrower than those for natural rivers due to space constraints in urban environments.

2.3. Time Marching Scheme

For numerically solving all governing equations, we adopt a four-stage third-order Strong-Stability Preserving Runge-Kutta (SSPRK3) time marching scheme (Durran, 2010). This numerical method offers two advantages: (a) It yields stable simulation results at relatively large time steps; (b) it minimizes the numerical diffusion during urban flood events where flow values vary abruptly (from low to high flows or vice versa) over relatively short periods (hours or at most days). The four stages of SSPRK3 for an Ordinary Differential Equation (ODE) of form $\partial_t V = \mathcal{F}(V)$ are:

$$\hat{V}^1 = V^n + \frac{1}{2}\Delta t \mathcal{F}(V^n), \tag{3}$$

$$\hat{V}^2 = \hat{V}^1 + \frac{1}{2}\Delta t \mathcal{F}(\hat{V}^1), \tag{4}$$

$$\hat{V}^3 = \frac{2}{3}V^n + \frac{1}{3}\left[\hat{V}^2 + \frac{1}{2}\Delta t \mathcal{F}(\hat{V}^2)\right], \tag{5}$$

$$V^{n+1} = \hat{V}^3 + \frac{1}{2}\Delta t \mathcal{F}(\hat{V}^3), \tag{6}$$

where Δt is the time step, and n and $n + 1$ superscripts denote the value in the current and the next time step, respectively.

Considering that in our modeling framework, $\mathcal{V}$ is water storage (m^3), the ODE represents the continuity equation with the general form of $\mathcal{F} = Q_{\text{in}} - Q_{\text{out}} + q_{\text{lateral}}\Delta x$, where Q_{in}, Q_{out}, and q_{lateral} are inflow, outflow, and lateral flow, respectively, and Δx is unit length along the flow direction. Each zone in our modeling framework solves this continuity equation with zone-specific inflow, outflow, and lateral flow components:

- Hillslope: No inflow; lateral flow is the generated surface runoff.
- Sub-network: No inflow; lateral flow is outflow from hillslope.
- Impervious: Inflow is outflow from urban hillslope; lateral flow is computed from precipitation and evaporation over the impervious area.
- Tributary pipes: Inflow is a portion of the outflow from the impervious zone based on the total number of tributary pipes; no lateral flow.
- Main pipe: No inflow; lateral flow is outflow from tributary pipes.
- Main channel: Inflow is streamflow from the upstream watershed (zero for headwater catchments); lateral flow is the combined outflow from sub-network and main pipe.

Table 1
AList of Model Parameters Estimated a Priori

Model component	Parameter	Data set/methodology
Hillslope	Length	LULC and NHDPlus
	Width	LULC and NHDPlus
	Slope	3DEP
	Roughness	Liu et al. (2019)
Storm-sewershed	Impervious area	NLCD Imperviousness
	BUSN	Chegini and Li (2022)
	Pipe data	Heilman (2022), UDFC (2016), Officials (2017)
Sub-network channel	Length	NHDPlus
	Width	Schwarz et al. (2018)
	Slope	NHDPlus
	Roughness	Decharme et al. (2019)
Main channel	Length	NHDPlus
	Bankfull depth	Schwarz et al. (2018)
	Bankfull width	Schwarz et al. (2018)
	Slope	NHDPlus
	Roughness	Decharme et al. (2019)

3. Parameter Determination and Hydrography Data Preparation

This section outlines the approaches to determining the model parameter and preparing associated hydrography data for application across watersheds in the contiguous United States. Here, "model parameters" refer to the static variables in the governing equations. Overall, our strategy for determining the model parameter values is to prioritize a priori estimation based on the publicly available datasets, and only calibrate those parameters that cannot be estimated easily from the existing data. Note that the boundary between these two lists of parameters may vary depending on the availability and quality of hydrography data.

In this study, hydrography and climate forcing data preparation primarily utilize HyRiver (Chegini et al., 2021), a suite of nine open-source Python libraries for various data processing purposes. Key libraries include PyNHD for retrieving hydrography data from the National Hydrography Data set Plus (NHDPlus) (U.S. Geological Survey, 2019), PyGeoHydro for accessing the hydrologic data from several hydroclimate data sources, and Py3DEP for obtaining topography data within the US through the 3D Elevation Program (3DEP) (U.S. Geological Survey, 2022).

In the following, we first describe in detail our strategy for estimating some parameters a priori, particularly those related to storm-sewersheds and BUSNs. We then briefly explain how we calibrate the rest of the parameters.

3.1. Parameters Estimation a Priori

First, we briefly describe the overall procedure for a priori estimation of parameters, then we provide more details on procedures related to storm-sewersheds and BUSNs.

3.1.1. Overall Procedure

Table 1 lists the parameters that can be estimated a priori, along with their data sources or methods, organized around each model component as outlined in Section 2.1.

The overall procedure to estimate these parameters is outlined in the following major steps for a watershed in the US:

1. Identify the watershed boundaries and corresponding river segments based on NHDPlus data using PyNHD. Within each watershed, PyNHD identifies the river segments on the main channel, and the rest are considered part of the sub-network channel (tributaries).

2. Divide the whole watershed area into two portions, natural and urban, based on the land use/land cover (LULC) (Dewitz, 2021) data at a 30-m resolution using PyGeoHydro. We further divide the urban portion into a number of storm-sewersheds. More details of storm-sewersheds delineation and parameter estimation are provided later.
3. We estimate the hillslope length within the watershed by dividing the total watershed area by the total length of all the tributaries and dividing again by two (hillslopes are distributed on both sides of sub-network channels). We assume the natural and urban portions in the watershed share the same hillslope length, based on the observation from the high-resolution LULC maps showing that the urban and natural surfaces are often interspersed along river segments.
4. Similar to Li et al. (2013), we parameterize all the natural hillslopes in the watershed in a lumped fashion, with the total width estimated as the sum of natural areas in the watershed divided by the hillslope length. The hillslope slope is estimated based on the topographic data (surface elevation and slope) at a 10-m resolution from U.S. Geological Survey (2022) using Py3DEP. The Manning's roughness coefficient is estimated using the LULC data set and a roughness-land cover type lookup table (Liu et al., 2019).
5. The major properties of the main and sub-network channels, such as length, bankfull width and depth, channel slope, etc., are derived from the attributes of the corresponding flowlines in the NHDPlus provided by Schwarz et al. (2018). The Manning's roughness coefficients for the channels are estimated following Decharme et al. (2019).

3.1.2. Scale-Adaptive Storm-Sewershed Delineation

For each storm-sewershed, we derive the corresponding BUSN and its physical properties using an algorithm developed by Chegini and Li (2022). This algorithm generates high-resolution BUSNs from publicly available datasets, such as street networks and LULC data, leveraging concepts from Graph Theory. A derived BUSN is essentially a network with flow directions (from one pipe to another), slope, and length attributes. Considering that the main purpose of this model is to represent BUSNs at large scales, we have devised an algorithm to systematically simplify a high-resolution BUSN into several simple pipe networks with equivalent discharge capacity (see Figure 2). Our algorithm consists of four main steps, details of which are provided subsequently:

1. Hydrologic conditioning of pipe elevations within a BUSN using a novel iterative algorithm based on the Depth-First Search (DFS) algorithm from graph theory.
2. Division of the BUSN into sub-BUSNs using a community detection algorithm from graph theory.
3. Enforcement of a single outlet for each sub-BUSN through the application of a novel iterative algorithm built upon DFS.
4. Simplification of each sub-BUSN into a single main pipe with several identical tributary pipes that connect laterally to the main pipe.

The BUSNs derived by the algorithm from Chegini and Li (2022) contain elevation data at pipe junctions. We ensure the hydraulic feasibility of the network based on minimum and maximum storm sewer pipe velocities of 2 (0.6 m/s) and 10 ft/s (3 m/s), respectively (TxDOT, 2019). These velocity limits ensure gravity-driven flow through BUSNs. We employ the Manning's equation Equation 1 to determine the minimum and maximum permissible pipe slope values for circular concrete pipes of various diameters with a Manning's roughness coefficient of 0.013, which are common in the United States (Heilman, 2022). Our calculations yield minimum and maximum slope values of 0.03% and 4.86%, respectively.

Starting from the pipe with the highest elevation, we navigate the BUSN using the DFS algorithm. In each iteration, we begin from a root pipe and traverse the network through all its connected pipes. During each traversal, we adjust the elevation of pipes to ensure their slopes remain within the permissible range. This process is repeated until all pipes have been visited, and their elevations adjusted, if needed.

For the second step, we adopt the Parallel Louvain Method (Staudt & Meyerhenke, 2016) to delineate sub-BUSNs, which are referred to as “communities” in graph theory. In the graph theory context, a network is a collection of nodes (pipe junctions) and edges (pipes) that connect the nodes, while a community is a subset of these nodes and edges. Nodes within a community are highly interconnected among themselves, but have fewer connections with nodes from other communities (Fortunato & Castellano, 2007).

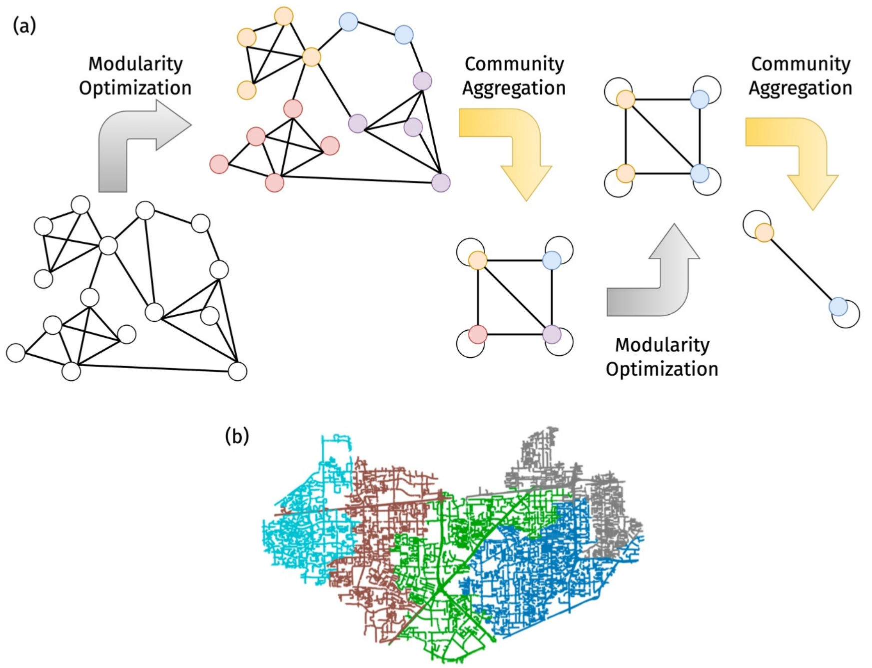

Figure 4. (a) Schematic representation of the Louvain community detection method (adapted from Blondel et al. (2008)). (b) Example of delineated sub-BUSNs using this community detection method.

As illustrated in Figure 4a, the Louvain method is a heuristic iterative approach consisting of two steps in each iteration: modularity optimization and community aggregation. Modularity, a value between −1 and 1, measures the density of connections between elements in a network. Modularity optimization maximizes the network's modularity by grouping elements between communities. Essentially, at each modularity optimization step, we categorize elements based on their connectivity (e.g., nodes with similar colors in Figure 4a). Community aggregation involves combining the elements of communities (e.g., nodes with the same color in Figure 4a) into a single element. These two steps are repeated until modularity is maximized, that is, when we can no longer categorize the nodes into smaller groups. Figure 4b depicts an example of delineated sub-BUSNs using this community detection method within an urban watershed in Houston, TX, where each color represents a sub-BUSN. In our framework, we use Networkit, an open-source Python package, for community detection (Staudt et al., 2015). This package implements the parallel Louvain method, which includes a multi-resolution modularity parameter. For this study, we set this parameter to 0.0002 through a trial-and-error approach.

After delineating sub-BUSNs, we enforce a single outlet for each sub-BUSN, as each sub-BUSN represents a storm-sewershed with exactly one outlet. Similar to the first step, we start from the pipe with the highest elevation and traverse the sub-BUSN using DFS, adjusting pipe elevations to ensure flows throughout the entire sub-BUSN are directed toward the pipe with the lowest elevation.

In our final step, within each delineated sub-BUSN, we categorize pipes into main and tributary classes based on their flow capacity using the Fisher-Jenks classification method (Jenks, 1977), with the number of classes set to two. We compute the flow capacity of each pipe using the maximum flow discharge through a circular pipe flowing at a height equal to 94% of its diameter, as given by the following equation (Chow, 1959):

$$Q_f = \frac{0.397}{n} D^{8/3} S^{1/2}, \tag{7}$$

where Q_f is the flow capacity, n is Manning's roughness coefficient, D is the pipe diameter, and S is the pipe slope.

We aggregate the lengths of all pipes in the main category to obtain the total length of the main pipe. For tributary pipes, we estimate their average length as the total length of all pipes in the tributary category divided by the number of street inlets. Pipe roughness and diameter values can vary between cities or regions. In the United

Table 2
Model Parameters That Require Calibration

Type	Parameter	Description	Range
Pervious	Sb_n	Water storage capacity of natural soil	10–2000 [mm]
	a	Shape factor of pervious areas	0–2 [−]
	γ	Surface/subsurface runoff partitioning coefficient	0–1 [−]
	k_b	Residence time of groundwater	0–0.14 [day^{-1}]
	Sb_c	Soil adjustment coefficient for urban pervious	0–1 [−]
Impervious	Sb_s	Max ponding storage capacity	0–10 [mm]
	G_p	Street inlets' spacing	1–100 [m]

States, the most common type of stormwater pipe is a circular concrete pipe with a 24 in. (0.6 m) diameter (Heilman, 2022). Therefore, we set the pipe diameter to 0.6 m for the main pipe and 0.45 m (18 in.) for the tributary pipes. We assume all pipes are made of concrete and use a Manning's roughness coefficient of 0.013.

For street inlets, we assume a rectangular shape of Type 13 (UDFC, 2016), which is common in the US, and obtain their geometrical properties from urban drainage manuals. In the US, street inlets with a length of up to 24 in. (0.6 m) are typical (Officials, 2017). Consequently, we assume all street inlets are 0.6 m long and 0.45 m wide.

Our proposed algorithm for delineating sub-BUSNs in watersheds is scale-adaptive and can be applied to any spatial unit, such as grid cells in grid-based models or catchments in subbasin-based models. The scale-adaptive nature of our algorithm is crucial for its application in large-scale modeling, allowing for efficient representation of urban stormwater networks across diverse spatial scales and urban environments.

3.2. Parameter Calibration

Seven parameters in our model require calibration rather than a priori estimation, as listed in Table 2. Note that the first four parameters are inherited from NRCS-PDM, and only the last three are added in this study. These parameters include:

1. Soil water storage capacity, Sb_n, ranging from 10 to 2000 mm. This parameter represents the maximum water storage capacity of natural soil, that is, soil that hasn't been impacted by human activities. Thus, after calibration, we apply this value to the natural hillslope.
2. Shape factor, a, ranging from 0 to 2. After calibration, we apply the same value to both hillslopes and storm-sewersheds in the same watershed.
3. Surface/subsurface runoff partitioning coefficient, γ, which has a theoretical range from 0 to 1. After its calibration, similar to a, we apply the same calibrated value for hillslopes and storm-sewersheds in the same watershed.
4. The residence time of groundwater in a linear reservoir, k_b, ranging from 0.0 to 0.14 day^{-1} according to Yao et al. (2020b). It is calibrated and applied similarly to a.
5. We assume the soil storage capacity for the storm-sewersheds in a watershed is a fraction of the soil storage capacity in its natural portion, since soils are usually compacted for construction purposes. Therefore, we introduce a new dimensionless parameter, Sb_c, to reflect this fraction value. The theoretical range of Sb_c is 0–1.
6. Ponding storage capacity for the impervious surface zone (mainly streets), Sb_s, represents the volume that the maximum depth of water the impervious zone can temporarily store. Based on reported values for the ponding storage from several studies, for example, American Society of Civil Engineers (1996); Brater (1968); Hicks (1944); Tholin and Keifer (1959), we set the range of this value to 0–10 mm.
7. The characteristic spacing intervals between street inlets, (G_p), is a parameter capturing the spatial density of inlets, assuming the inlets are distributed uniformly along the streets. For determining the range of G_p, we carried out a sensitivity analysis (SA) by systematically increasing this parameter from 1 to 1,000 m while keeping the other model parameters fixed. The results of our analysis show that values beyond 100 m do not change the model results noticeably, thus we set the range of G_p to 1–100 m.

For calibration, we use the Tree-Structured Parzen Estimator (TPE) (Watanabe, 2023) algorithm that is a Bayesian optimization algorithm with efficient nonlinear constraint handling. TPE is available via Optuna (Akiba et al., 2019), an open-source Python package. Note that the main objective of this study is to simulate urban floods better. We use Peak-Weighted Root Mean Squared Error (PWRMSE) (USACE, 2022) at the daily scale as the objective function in TPE. PWRMSE assigns weight values of greater than one to streamflow values larger than the mean observed streamflow. It implicitly compares the magnitude, volume, and timing of peak flows between two hydrographs (USACE, 2022). We compute PWRMSE as follows:

$$\text{PWRMSE} = \sqrt{\frac{1}{N}\sum_{i=1}^{N}\left[\left(Q_o^i - Q_s^i\right)^2 \frac{Q_o^i + \overline{Q_o}}{2\overline{Q_o}}\right]} \tag{8}$$

where N is the number of streamflow values, and Q_s, Q_o, and $\overline{Q_o}$ are simulated, observed, and the mean observed streamflow values, respectively.

In addition to PWRMSE, we adopt Kling-Gupta Efficiency (KGE) (Gupta et al., 2009) at the daily scale and percentage bias (PBIAS) at the annual scale as constraints in TPE. KGE is a comprehensive metric that evaluates model performance by considering three components: correlation, bias, and variability. It ranges from $-\infty$ to 1, with higher values indicating better model performance. A KGE value of 1 represents perfect agreement between simulated and observed values, while a value of -0.41 indicates that the model performs as well as using the mean of the observed data. KGE values below -0.41 suggest that the model's predictive skill is lower than that of the observed mean (Knoben et al., 2019). PBIAS at the annual scale measures the model's performance in predicting the observed annual water balance and ranges from -100% to 100%. A PBIAS of 0% indicates perfect agreement between simulated and observed annual volumes, with positive values indicating overestimation and negative values indicating underestimation by the model.

We set the minimum acceptable KGE value to 0.5 and the maximum acceptable absolute PBIAS value to 15%. These constraints guide the optimization algorithm toward results that have acceptable KGE and PBIAS values while minimizing errors in peak flow magnitude and timing predictions.

4. Model Demonstration

The aforementioned modeling and parameterization strategies can be implemented using any programming language or technique. In this study, we implement them in the form of a watershed-scale urban hydrologic model in Python, utilizing exclusively open-source libraries. Figure 5 illustrates technical details of our model. We apply the model to the selected case studies, as detailed in this section.

4.1. Case Studies and Data

For demonstration, we select nine representative watersheds within the Houston metropolitan area, Texas, as listed in Table 3. The selection criteria mainly include the availability of observed daily streamflow data and varying levels of urban development. Figure 6 shows the watersheds that match our criteria, including two natural watersheds and seven urban watersheds with low, moderate, and high urban imperviousness. In the Houston area, separate sewage systems are dominant (EPA, 2018). Based on the Texas wastewater outfalls data set (TCEQ, 2023), the streamflow at the outlets of these nine watersheds is mostly affected by stormwater sewage only, that is, not affected by the sanitary sewage discharge from wastewater treatment plants. The drainage areas of these watersheds range from 24 to 302 km^2, sufficiently small so we can focus on land processes instead of riverine processes. Table 3 summarizes basic information for these nine watersheds. The watersheds vary in urban imperviousness and drainage areas, providing a robust testbed for evaluating the model's performance.

We set our study period to 2003–2020 mainly based on the data availability, particularly daily observed streamflow data from the United States Geology Survey (USGS) stations at the watershed outlets. Our model can run at both daily and sub-daily time steps. In this study, we run the model at the hourly time step to better capture flood peaks. The climate forcing data are from the North American Land Data Assimilation System project Phase 2 (NLDAS-2) (Xia et al., 2012) data set. We retrieve hourly precipitation and potential evapotranspiration (PET) data from NLDAS-2 using the PyNLDAS2 (Chegini et al., 2021) Python package. NLDAS-2 data are provided in regular grids with a 25 km resolution, so they are remapped to the watershed scale in this study. The other static input data are prepared using the HyRiver libraries as outlined in Section 3.1.

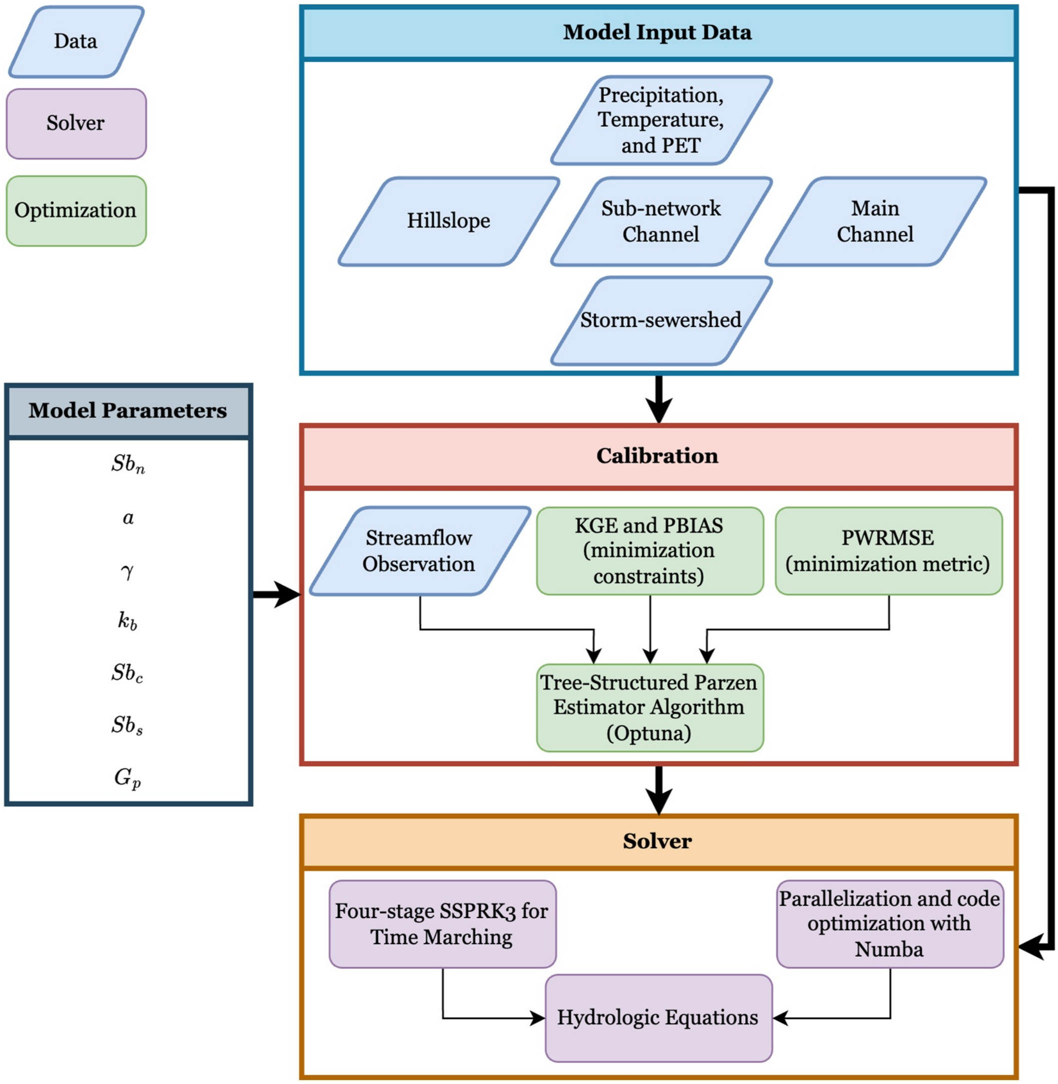

Figure 5. A diagram demonstrating technical details of our proposed modeling framework.

4.2. Calibration and Validation

We calibrate our model using 70% of observation data (2003–2015) and validate it with the remaining 30% (2016–2020). Considering the daily timescale of the streamflow observations, we convert the simulation results from hourly to daily for calculating the model performance metrics. Table 3 also lists the daily KGE and PWRMSE values in the validation period (2016–2020). Results show that our model effectively captures the daily streamflow across a range of urban imperviousness, with the daily KGE values between 0.53 and 0.86 and daily PWRMSE values ranging between 13 and 58 mm day^{-1}. Knoben et al. (2019) suggested that KGE values above 0.3 can be considered acceptable in hydrological modeling. Our KGE values are well above this threshold, indicating excellent model performance across all watersheds. In the urban watersheds, the peak flows are substantially higher than those in the natural watersheds. However, for PWRMSE, there appear to be no obvious differences between the urban and natural watersheds, suggesting that our model has effectively captured the effects of BUSN and storm-sewersheds on peak flows.

We choose 2017, the year when Hurricane Harvey made landfall, to illustrate the simulated daily streamflow, as shown in Figure 7. Note the unit for streamflow is mm/day to minimize the impacts of different watershed sizes. It appears that the model captures the magnitudes and timing of peak flows reasonably well.

10.1029/2024WR037268

Table 3
Basic Information for the Nine Selected Watersheds in Houston, TX

Station ID	A^{*a}	$I^{\dagger b}$	$SS_n^{\ddagger c}$	$T^{\S d}$	KGE[‖e]	PWRMSE[‖e]
08068740	302	–	–	0.2	0.75	23.70
08071000	277	–	–	0.2	0.67	29.90
08072300	172	16	6	2.8	0.74	13.36
08068450	88	36	7	3.3	0.70	32.85
08072760	49	45	6	2.9	0.52	57.15
08076500	75	50	11	5.1	0.72	19.08
08075730	24	54	4	2.0	0.82	24.43
08075770	48	60	7	3.5	0.80	29.71
08075000	262	64	11	4.9	0.86	17.51

Note. All abbreviations in this table are only for the purpose of this table and are not used elsewhere. [a]$^*A$ denotes the total area of the watershed. [b]$^\dagger I$ denotes the percentage of imperviousness in the watershed. [c]$^\ddagger SS_n$ denotes the number of storm-sewersheds in the watershed. [d]$^\S T$ denotes runtime based on hourly simulations (2003–2020). [e]‖KGE and PWRMSE are based on daily streamflow (2016–2020).

We further examine the magnitudes of simulated annual maximum daily floods (AMFs). Figure 8 compares the observed and simulated AMFs from 2003 to 2020. Note that, in Figure 8, we simply rank the AMFs based on their magnitude without assigning the return periods. This is because the return periods calculated only based on the 18 years of flood records can be very misleading. For instance, the return period of the 2017 flood (caused by Hurricane Harvey) can be as high as 1,000 years or more (van Oldenborgh et al., 2017). Overall, the model captures small to large flood peaks, as shown in Figure 8.

Both Figures 7 and 8 show noticeable underestimation of peak flows, particularly during hurricanes such as Harvey. Such underestimation can be attributed to two possible reasons:

1. There are noticeable biases in the precipitation data, particularly during extreme rainfall events like Hurricane Harvey. M. Chen et al. (2020) compared four different precipitation datasets during Hurricane Harvey and showed that the Multi-Radar Multi-Sensor system (MRMS) provided the best data quality, which nevertheless still contains underestimations of the highest rainfall intensity during the event.
2. The NRCS-PDM runoff scheme centers on saturation excess runoff, which occurs when the soil becomes fully saturated and cannot absorb additional water. However, this approach tends to underestimate AMFs by neglecting infiltration excess runoff, which happens when rainfall intensity exceeds the soil's infiltration capacity. In reality, both mechanisms contribute to flood peaks during extreme rainfall events (Li & Sivapalan, 2011; Li et al., 2013; Wang, 2018; H. Wu et al., 2014; Yao et al., 2020a). The infiltration excess process is particularly relevant during high-intensity

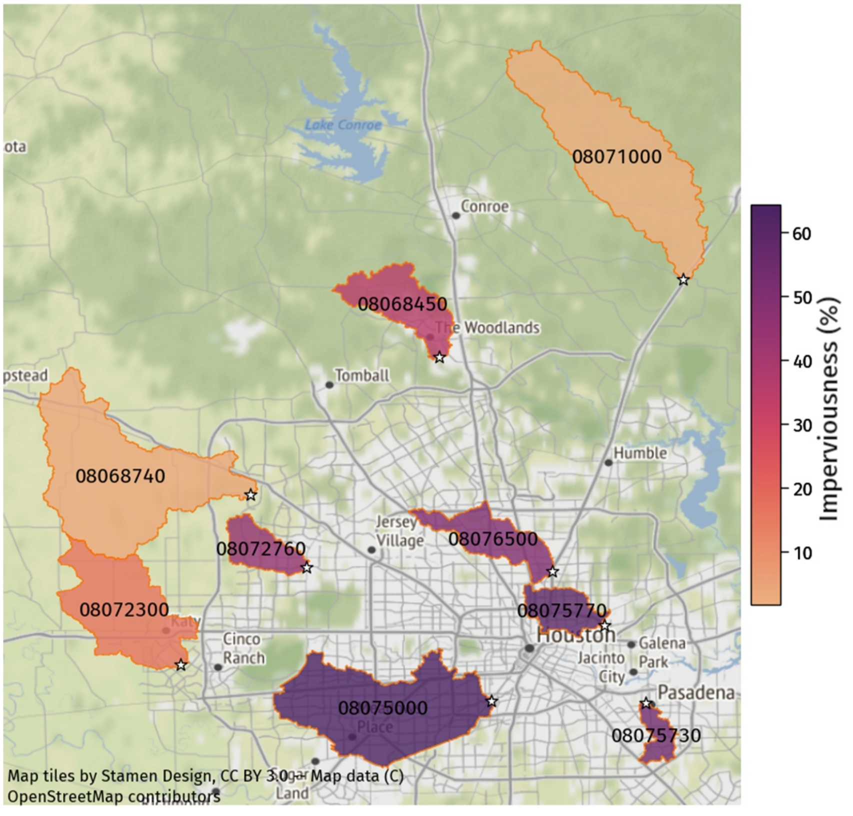

Figure 6. Selected watersheds in Houston, Texas, with their United States Geology Survey station identifiers.

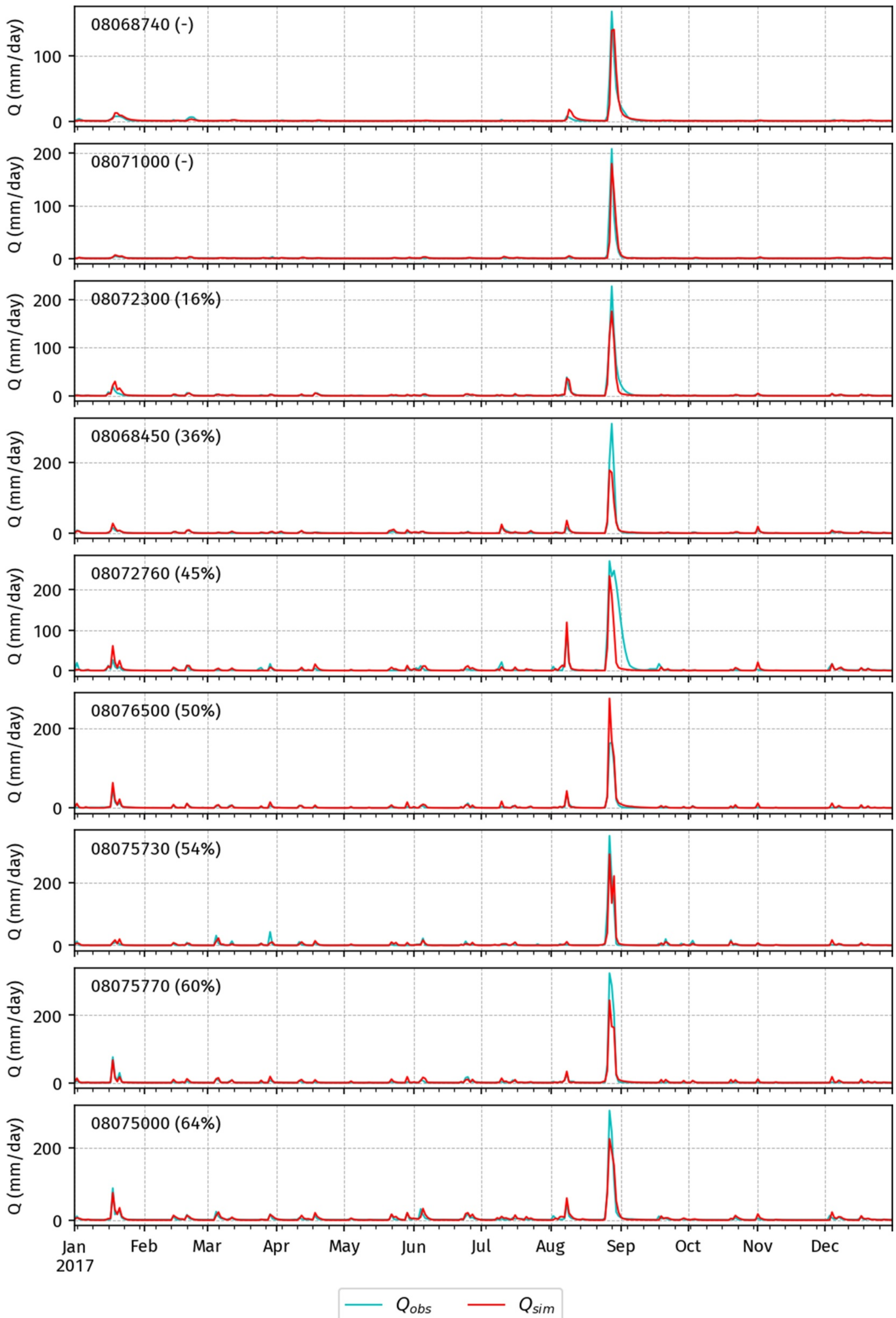

Figure 7. Observed and simulated daily streamflow for 2017. The numbers in the parentheses are imperviousness levels.

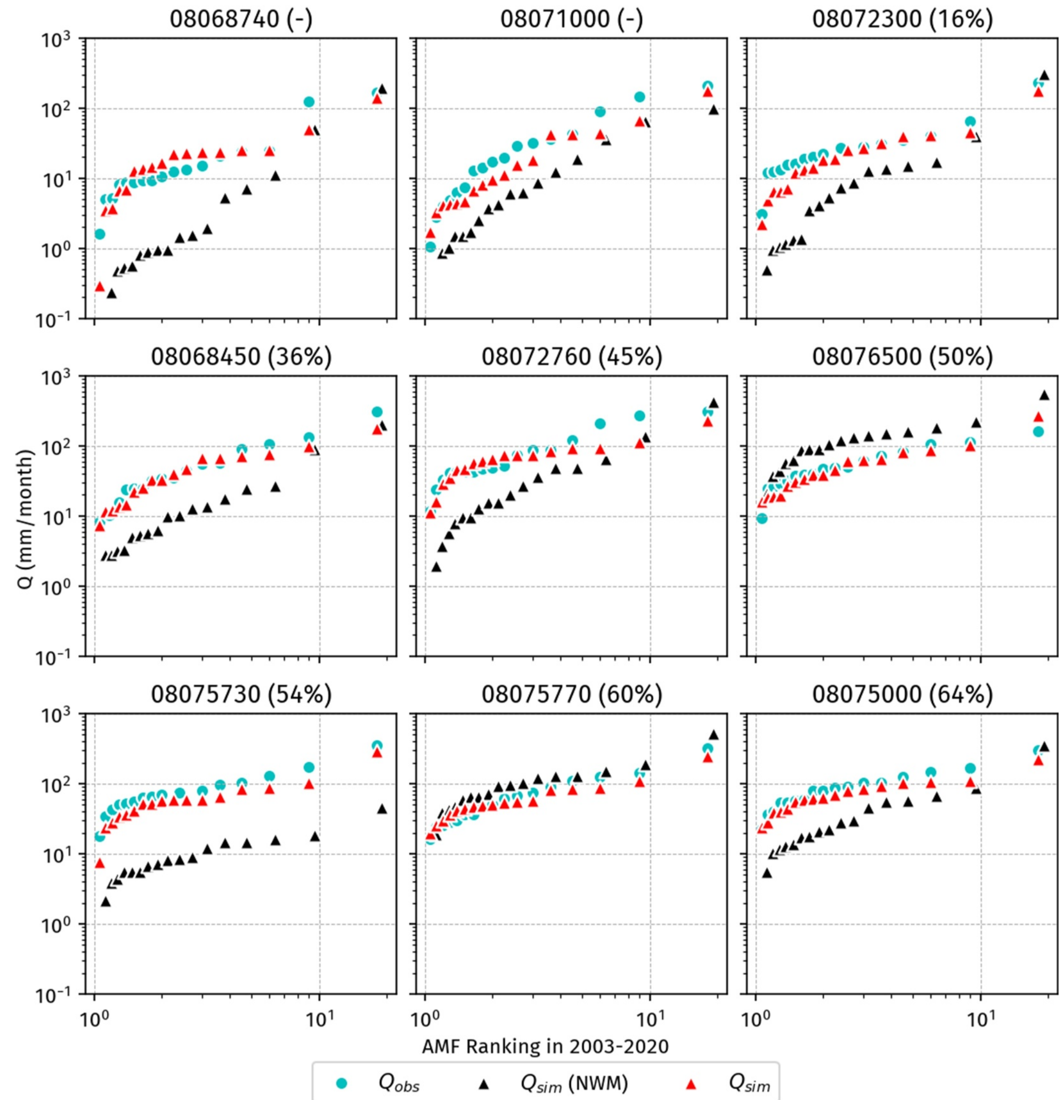

Figure 8. AMFs in 2003–2020 from the observed streamflow (Q_obs) and simulated from our model (Q_sim) and NWM ($Q_sim(NWM)$), respectively. The numbers in the parentheses are imperviousness levels.

precipitation events like Hurricane Harvey, potentially leading to faster runoff generation and higher peak flows. Addressing these limitations is beyond the scope of this study and left for future improvements.

A plot of mean monthly streamflow, or regime curve, is usually a good signature for the model's capacity in simulating watershed seasonal water balance (Tian et al., 2012). Figure 9 depicts the simulated and observed regime curves over the validation period. Overall, the model reasonably captures the streamflow seasonal variations and, hence, seasonal water balance. The model underestimates peak monthly flows at Stations 08068740 and 08072760, likely due to the biases in either the NLDAS2 precipitation or USGS streamflow observations during the hurricanes.

4.3. Comparison With National Water Model

We compare our model simulation with retrospective simulation results of the National Water Model (NWM) version 3 (Cosgrove et al., 2024). NWM is a continental-scale hydrologic model developed by the U.S. National Oceanic and Atmospheric Administration (NOAA) for forecasting streamflow and inundation over the United States. NWM has 14 calibrated parameters, does not include BUSNs, uses Analysis of Record for Calibration (Fall et al., 2023) forcing data, and provides retrospective results from 1979 to 2023 at an hourly timescale

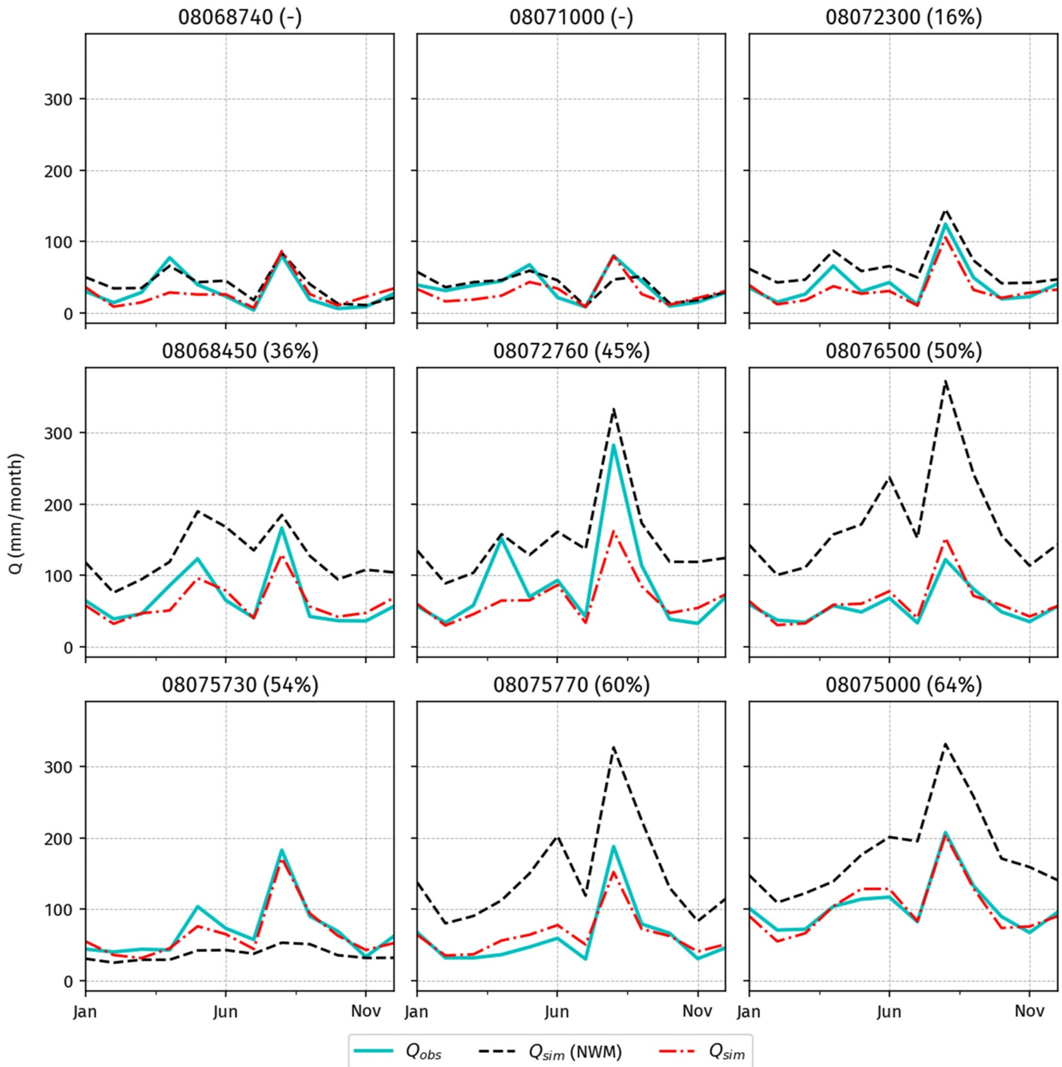

Figure 9. Mean monthly streamflow in 2016–2020 from the observed streamflow (Q_obs) and simulated from our model (Q_sim) and NWM ($Q_sim(NWM)$). The numbers in the parentheses are imperviousness levels.

(National Oceanic and Atmospheric Administration, 2024). This comparison is crucial for assessing our model's fidelity against a well-established, large-scale operational model.

Figure 8 indicates that our model produced apparently smaller biases in simulating AMFs at most watersheds, except for Station 08075770, where both models perform equally well. The superior performance of our parameter-parsimonious model in urban areas, despite using only seven parameters compared to the NWM's 14, demonstrates the effectiveness and efficiency of our parameterization strategy for urban areas. This comparison not only validates the performance of our model but also underscores the importance of incorporating BUSNs in large-scale urban hydrological modeling.

Figure 9 compares simulated mean monthly streamflow from both models. It appears that, in terms of capturing seasonal water balance, our model's performance is comparable to NWM at the natural watersheds, but much better at most urban watersheds. Note that, NWM significantly underestimated AMFs at most stations except for Station 08076500 and 08075770, but these underestimations can not be explained by the biases in simulated seasonal water balance, that is, mean monthly streamflow, shown in Figure 9. Therefore, our model outperforms NWM in terms of both flood peaks and seasonal water balance.

Recall that our model has seven and five parameters for calibration over urban and natural watersheds, respectively, much less than the 14 parameters calibrated in NWM. These comparisons thus demonstrate the effectiveness of our parameterization strategy and underscore the importance of incorporating BUSN in urban hydrologic modeling at the watershed and larger scales.

4.4. Model Runtime

We enhance the model's computational efficiency in three ways: (a) Network-level representation of stormwater pipes, (b) selecting computationally efficient yet accurate enough governing equations for different hydrological processes; (c) parallelization using Numba (Lam et al., 2015) which allows parallel computing on a multi-CPU standard PC as well as large high-performance computing clusters. We record our model's runtime for the nine watersheds in 2003–2020 at an hourly time step, as listed in Table 3. The simulations are conducted on an Apple Mac Studio with an M2 chip featuring 12 CPU cores. For the two natural watersheds, each simulation takes only 0.2 s. For the seven urban watersheds, the runtime varies from 1.8 to 4.5 s, mainly correlating with the number of storm-sewersheds and the imperviousness percentage. The more complex the urban structure, the longer the runtime. For instance, watersheds with a higher number of storm-sewersheds and greater imperviousness, such as 08075000 and 08076500, exhibit longer runtime (4.3 and 4.5 s respectively). Importantly, even for the most complex watersheds in our study, the runtime remains under 5 s. This demonstrates the remarkable computational efficiency of our model across varying levels of watershed complexity.

5. Parameter Sensitivity Analysis

5.1. Methodology

To study the importance of parameters, we carry out a parameter sensitivity analysis (SA) using the Morris method (Ruano et al., 2012) from the SAlib Python package (Iwanaga et al., 2022). This method is a one-factor-at-a-time global SA approach and is one of the most common methods for SA of hydrological model parameters (e.g., King & Perera, 2013; Song et al., 2015; S. Wu et al., 2022). Essentially, it takes a permissible range of model parameters as input, generates random samples of the model parameters, and evaluates the distribution of Elementary Effects (EE) of model parameters on an objective function. EE is a measure of changes in the model output due to perturbations of one parameter. The Morris method generates two outputs: the mean of the absolute values of EEs, μ^*, and the standard deviation of the EEs' distribution, σ. A higher μ^* indicates the higher influence of a parameter, whereas a higher σ translates to a higher degree of interactions between a parameter and the others. In other words, large σ values imply that the model's performance is sensitive to the combined effects of multiple parameters rather than an individual parameter. For convenience, we denote μ^* and σ as the influence and interaction indicators, respectively (see Figure 10). In this study, we focus on the model's capacity to simulate flood peaks in urban watersheds, so we measure the sensitivity of model parameters by considering PWRMSE as the performance metric.

5.2. Results and Implications

Figure 10 shows the results of the Morris SA and reveals distinctive parameter behaviors across varying levels of watershed imperviousness. Sb_n (soil storage capacity) emerges as the most influential parameter, exhibiting both high μ^* and σ values, indicating strong overall impact and significant non-linear or interaction effects. G_p (street inlets' spacing) demonstrates increasing influence with imperviousness, suggesting its critical role in highly urbanized watersheds. a (shape factor) and γ (runoff partitioning coefficient) display moderate influence with notable interaction effects, particularly in less impervious settings. Sb_c (soil adjustment coefficient) and k_b (groundwater residence time) exhibit moderate overall influence, with varying degrees of non-linear interactions. Interestingly, Sb_s (max ponding storage capacity) shows minimal impact across all imperviousness levels. This low sensitivity is likely due to similar engineering practices invoked during urban development in the same region, such as soil compaction or impervious infrastructure construction.

The sensitivity analyses have several implications: (a) The varying sensitivity of parameters across various imperviousness levels indicates the model can capture the transition from natural to urban environments. (b) Sb_n and G_p need to be carefully calibrated or estimated, particularly for urban watersheds. (c) Sb_s can be potentially set as a default value for regional-scale applications, or calibrated directly at a regional scale instead of separately at the watershed scale.

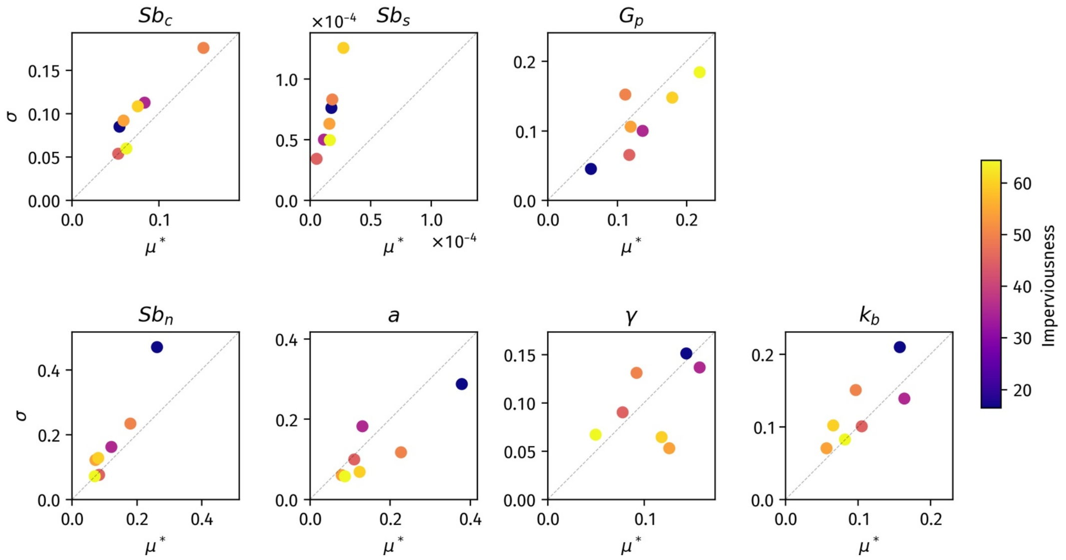

Figure 10. Sensitivity analysis of the model parameters. μ^* is the influence indicator. σ is the interaction indicator. Each point represents one watershed.

6. Further Analyses

This section provides in-depth analyses to (a) examine whether our model is getting the right answer for the right reasons, and (b) gain deeper insights into the impacts of BUSN on urban flood reduction. We begin by thoroughly examining the Hurricane Harvey event across nine watersheds. We then quantify BUSN's flood reduction effects across different flood intensities and urban settings.

The flood event caused by Hurricane Harvey lasted from August 27 to 29, 2017. We simulate this event with two different configurations: With $G_p = 0$, that is, assuming no BUSN, and with $G_p = 5\ m$. Comparing these two configurations helps quantify the net effects of BUSN. Figure 11 shows the results for these two configurations during Hurricane Harvey at all nine watersheds. As expected, there is no noticeable difference in the first row, where the three watersheds are either natural or have small imperviousness. However, in the other watersheds, BUSNs at least noticeably reduce the magnitude of flood peaks. In terms of timing, BUSN does not appear to delay the timing of flood peaks significantly.

Figure 11 also suggests that, for multi-day flood events like Hurricane Harvey, the flood reduction effect is stronger for the first flooding day (i.e., August 27th) than for the later days. The reason is that the designed BUSN capacities for interception and transient storage of excess stormwater are largely reached during the first day, leaving little capacity for subsequent days. Therefore, the flood reduction effect has been weakened in the later stage of multi-day flood events. This phenomenon is more pronounced for the watersheds with high imperviousness (hence more BUSN capacities), for example, those corresponding to the 08075730, 08075770, and 08075000 stations.

The flood reduction effects observed in Figure 11 can be better understood by examining the underlying processes, which our physically-based model enables us to quantify and visualize in Figure 12. Figure 12 depicts the major processes driving streamflow variability in watersheds 08075730, 08075770, and 08075000 during Hurricane Harvey: rainfall variability, overflow from the impervious zone, and BUSN outflow. Impervious zone overflow responds more directly to rainfall variations and exhibits much higher temporal variability than BUSN outflow. Note that the high temporal variability in impervious zone overflow only partially propagates to that of streamflow, due to the channel routing processes in the sub-network and main channels. BUSN outflow exhibits a more dispersed pattern, mainly due to the routing process through the BUSN pipes with very mild slopes. BUSN essentially offers substantial buffering of stormwater, which eventually helps reduce flood peaks. This is consistent with the fact that one of the major purposes of BUSN is the safe, gradual conveyance of stormwater toward the receiving rivers. Additionally, we can discern from Figure 12 that the impervious overflow contributes the most on the first two days with the most precipitation (August 27th and 28th), whereas the BUSN outflow

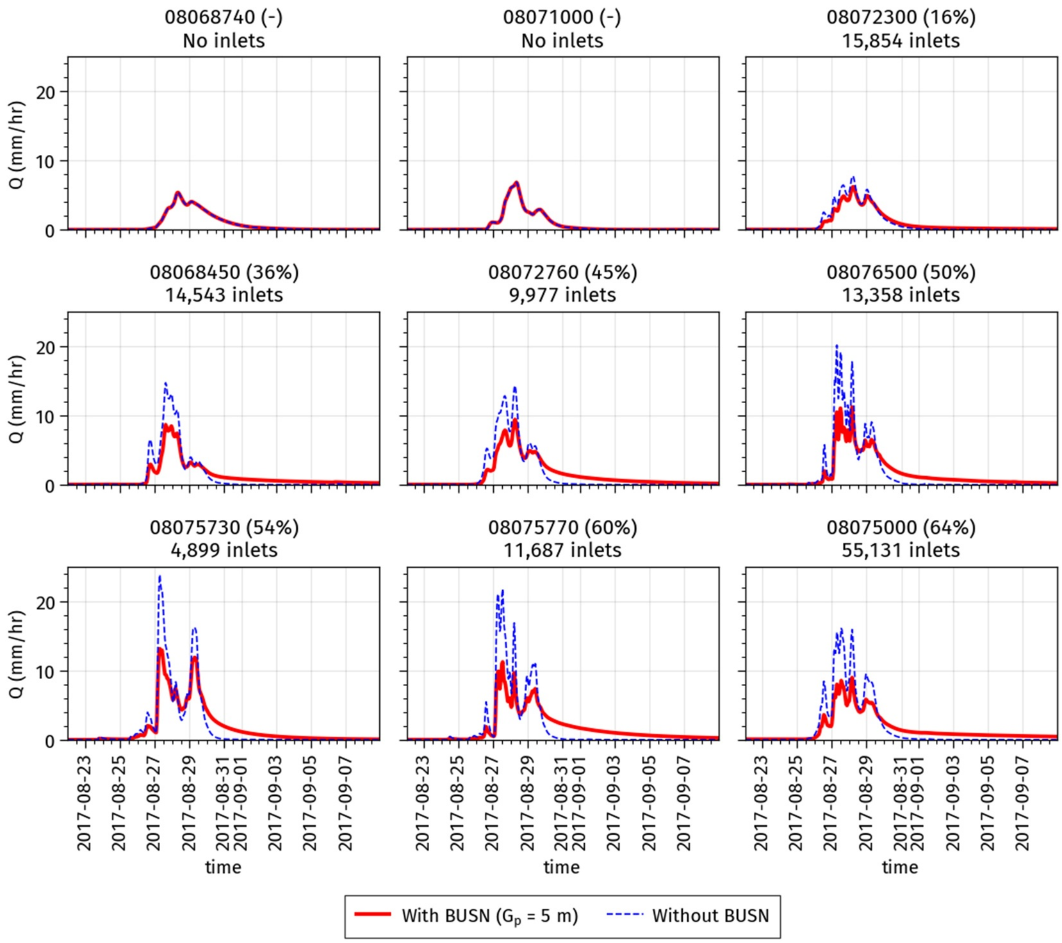

Figure 11. Impact of BUSNs on hourly hydrographs during Hurricane Harvey.

contributes the most on the last day of the rainfall event (August 29th). This can be attributed to the fact that when the precipitation reaches its peak, due to the limited interception capacity of BUSNs, most surface runoff becomes impervious overflow. However, as the rainfall subsides and surface runoff decreases, the contribution from the BUSN outflow increases due to the delayed release.

We further analyze the flood reduction effect of BUSNs by measuring the peak reduction percentage due to BUSNs for the nine watersheds during Hurricane Harvey (August 27th to 29 August 2017), as shown in Figure 13. We compute the flood reduction percentage as follows:

$$\gamma = \frac{Q_{\mathrm{pwo}} - Q_{\mathrm{pw}}}{Q_{\mathrm{pwo}}} \times 100 \tag{9}$$

where γ, Q_{pwo}, and Q_{pw} are peak reduction percentage, peak discharge without BUSN during a rainfall event, and peak discharge with BUSN during the same event, respectively. Overall, the flood reduction effect increases with the imperviousness and interception capacity of BUSNs, up to 50%. This effect, nonetheless, weakens substantially from August 27 to 28 and then 29, since the transient storage capacity of BUSNs has been reached and less and less stormwater can be taken by the BUSNs.

While the Hurricane Harvey event analyses provide valuable insight into the internal functioning of our model, it is important to understand BUSN's hydrologic functions across various levels of flood intensities and urban imperviousness. Figure 14 contrasts the flood-reduction effects over three storm events of different magnitudes: Tropical Storm Imelda (August 2019, low intensity), Memorial Day Flood (May 2015, medium intensity), and

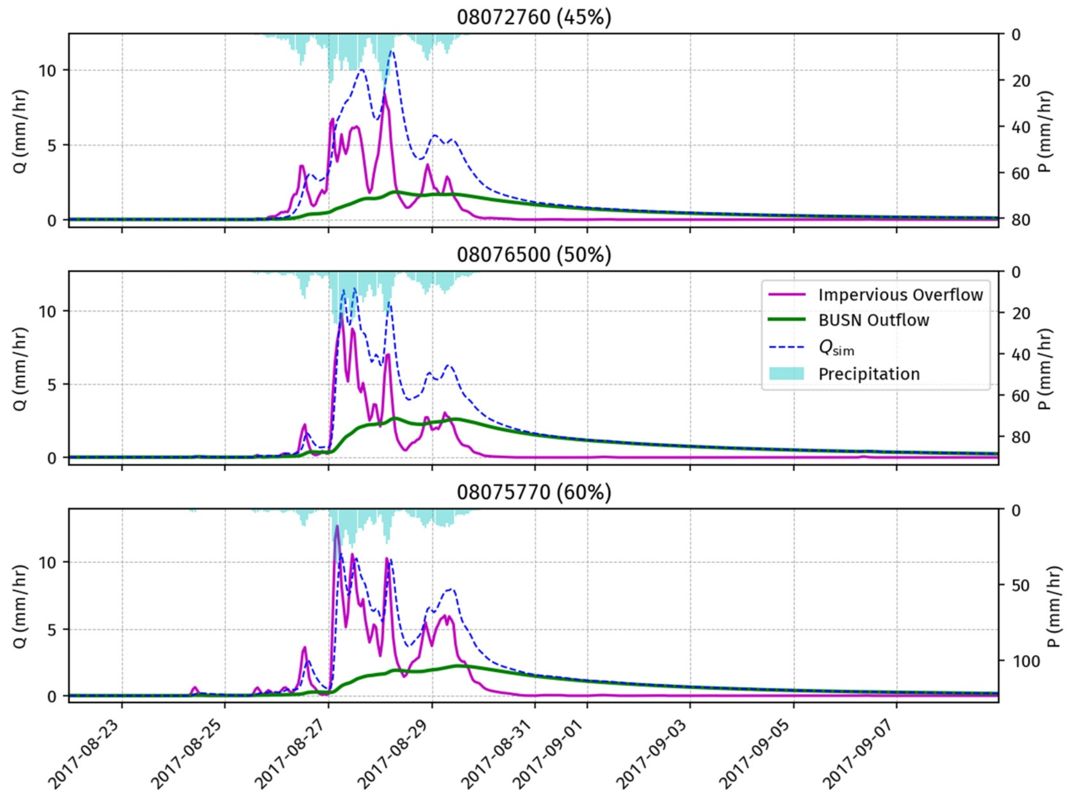

Figure 12. Interplay between hourly rainfall, impervious zone overflow, BUSN outflow during Hurricane Harvey at three watersheds with high imperviousness.

Hurricane Harvey (August 2017, high intensity). For clarity, we focus on three watersheds with varying imperviousness levels: 08072300 (16%), 08072760 (45%), and 08075000 (64%). For each case, we systematically decrease the inlet spacing (G_p) from 100 to 1 m, and determine the peak reduction percentage (γ) during each flood event based on the corresponding simulations. We note that inlet spacing refers to the distance between inlets, thus, by reducing this distance, the total number of inlets in a watershed increases, that is, lower inlet spacing corresponds to higher BUSN interception capacity.

Figure 14 demonstrates that γ varies between 5% and 70%, as expected, by increasing the inlet spacing, the peak reduction capacity of BUSN decreases. Moreover, for all stations, there is a decrease in flood reduction capacity as the flood intensity increases. However, this decrease in the reduction capacity becomes more pronounced as the imperviousness decreases. For example, the maximum γ value under these three flood events for stations

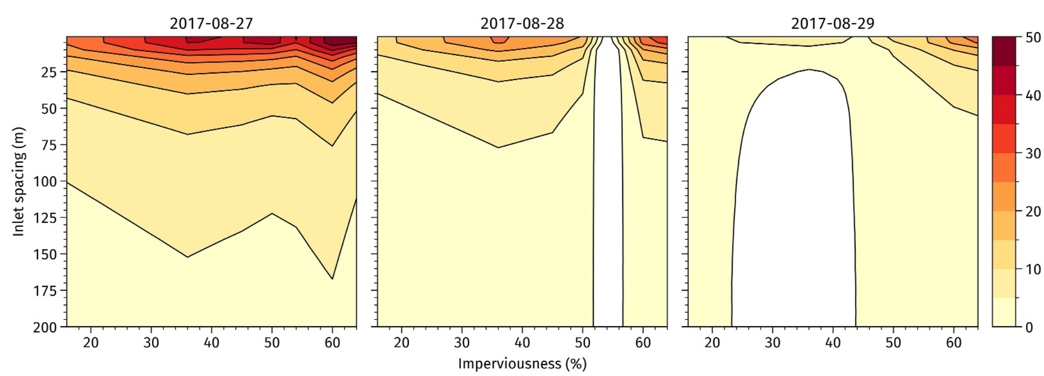

Figure 13. Changes in flood reduction effect of BUSNs at different levels of imperviousness and inlet spacing during Hurricane Harvey.

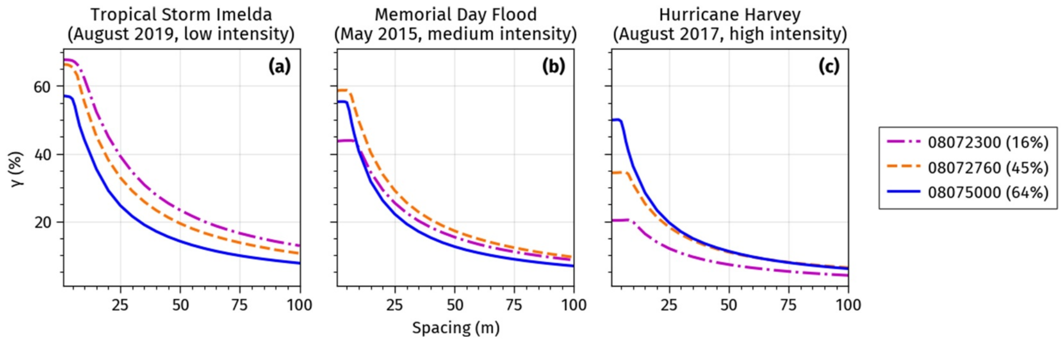

Figure 14. Comparison of peak reduction percentage (γ) for three urban watersheds with United States Geology Survey station IDs of 08072300, 08072760, 08075000 that have different imperviousness levels under three storm events with various intensities: (a) Tropical Storm Imelda (August 2019, low intensity), (b) Memorial Day Flood (May 2015, medium intensity), and (c) Hurricane Harvey (August 2017, high intensity).

08075000 (64% imperviousness), 08072760 (45% imperviousness), and 08072300 (16% imperviousness) varies between 50%–60%, 35%–70%, and 20%–70%, respectively. This can be attributed to the availability of more space for placing inlets in watersheds with larger impervious areas. Additionally, the figure reveals that watersheds with more natural areas (less imperviousness values) have a slightly higher flood reduction effect for lower-intensity flood events. However, as the flood intensity increases, the effect of BUSNs on flood reduction becomes more pronounced. The range of γ for different inlet spacing values during the low-intensity flood event is about 45% for all three watersheds. However, as the flood intensity increases, this range decreases, and for Hurricane Harvey, it reaches 40%, 25%, and 15%, for stations 08075000 (64% imperviousness), 08072760 (45% imperviousness), and 08072300 (16% imperviousness), respectively. This can be attributed to the quicker discharge of stormwater to BUSNs in comparison to the retention and infiltration of stormwater in natural parts of watersheds.

Moreover, Figure 14 shows an interesting threshold behavior around the spacing value of 10 m. When the spacing value is less than 10 m, the γ values either remain at the maximums (e.g., during Memorial Day Flood and Hurricane Harvey) or decrease gradually with increasing spacing (e.g., during Tropical Storm Imelda). When the spacing value is larger than 10 m, there is a sharp decrease in γ with increasing spacing. This threshold behavior can be attributed to the shifting dominance of BUSNs' interception capacity and conveyance capacity when inlet spacing varies. Note that the interception capacity increases with decreasing spacing (higher inlet intensity). When the spacing is relatively sparse, the interception capacity dominates the overall flood reduction effect. When the spacing is sufficiently small, the BUSNs' conveyance capacity starts to dominate, and hence increasing the interception capacity is no longer effective.

Collectively, Figures 11–14 suggest that using our model, we are able to yield similar, quantitative understandings as previous studies, validating its physical basis. More importantly, our model's computing efficiency allows for comprehensive numerical experiments, generating new insights, including (a) the non-linear, threshold relationship between inlet spacing and flood reduction, (b) the temporal dynamics of BUSN's functions at event scale, (c) comparative analyses across various flood intensities and watershed imperviousness levels.

7. Discussion

Thus far, we have filled the knowledge gap between large-scale hydrologic models and hydraulic-based models by introducing and demonstrating a new modeling and parameterization strategy. This new strategy centers on a network-level representation of stormwater pipes that can sufficiently well capture major hydrologic functions of BUSNs, namely interception, conveyance, and transient storage of urban runoff. This approach allows for explicit representation of BUSNs in watershed-scale modeling, overcoming a significant limitation in previous large-scale modeling.

Our BUSN parameterization benefits from several Graph-Theory-based algorithms, such as DFS and community detection. A typical urban watershed can be divided into a number of storm-sewersheds, each underpinned by a sub-BUSN intercepting and conveying urban runoff within a storm-sewershed to a single outfall in a dispersed fashion (hence flood reduction). The number of storm-sewersheds is not arbitrary but rather varies with the imperviousness level, that is, scale-adaptive. All the parameters related to storm-sewershed and BUSN are estimated a priori without losing much accuracy, as shown in our model demonstration (4). Such a parameterization accounts for local-scale urban hydrologic heterogeneity within a watershed without introducing additional parameters. It is just parsimonious and transferable, at least over watersheds in the whole contiguous United States. The scale-adaptive sub-BUSN and storm-sewershed delineation, combined with a priori estimation of BUSN parameters, presents an effective solution to the long-standing challenge of data scarcity in urban hydrologic modeling.

The aforementioned network-level presentation and parameterization help reduce computational burden in two ways: (a) It avoids computations at individual pipes and their interactions; (b) it avoids hydraulic-based governing equations, which typically invoke much more calculations than hydrologic equations. These computational features, combined with the time marching and parallel computing methods, lead to high computational efficiency in our model, yielding an important improvement over existing hydraulics models.

Our model holds promising potential for various applications, including but not limited to:

1. Advancing scientific understanding: As illustrated in Section 6, the model serves as a powerful tool to generate new insights into the nonlinear urban hydrologic responses and their interactions.
2. Climate change impact assessment: The model's computational efficiency makes it valuable in long-term simulations in urban watersheds, which is necessary for accessing existing urban flood-mitigation infrastructure under various climate change scenarios.
3. Decision support for urban planning and management: The model can play a crucial role in optimizing BUSN design and urban planning strategies. For example, a reasonable balance between interception, conveyance, and transient storage capacities can lead to a more cost-effective stormwater management system.

There are, nevertheless, several limitations in our model, including but not limited to (a) Our model incorporates less detailed process descriptions than hydraulic-based models. Hence, it should be used as a complementary instead of replacement of hydraulics-based models, particularly under circumstances where local-scale, highly process-based modeling capacity is necessary. (b) The model does not include sanitary sewage or pollutants. So it cannot be used to conduct water quality analysis in urban settings. (c) It only simulates peak flows, but not inundation dynamics. (d) It does not explicitly include other urban infrastructure such as stormwater detention/retention ponds, low-impact developments, etc.

To overcome some of these limitations, possible future directions are (a) Coupling our model with an existing inundation model to simulate urban inundation dynamics, (b) Extending our model to include the other urban infrastructure, (c) Incorporating our model into a large-scale hydrologic modeling framework for simulating urban hydrologic processes at the regional and larger scales.

8. Conclusion

In this study, we have introduced an urban hydrologic modeling framework at the watershed scale that centers on a network-level representation of BUSNs and a corresponding parameterization strategy based on graph theory. Based on such strategies, we have developed a watershed-scale model that is physically based, computationally efficient, and parameter parsimonious. We successfully validated the model against observed daily streamflow and compared it with the National Water Model v3 over nine representative watersheds with a range of imperviousness levels and drainage areas. We also showed that, although our model has some limitations, it can be used to generate interesting new insights, as outlined in Section 7.

Our model's robust performance across different spatial and temporal scales, parsimonious parameterization, and high computing efficiency make it a valuable tool for improving our predictive understanding of urban hydrologic processes and urban planning and flood management at the watershed and larger scales.

Data Availability Statement

The code that we developed for producing the results presented in this manuscript is available at Chegini et al. (2024).

Acknowledgments

T. Chegini and H.-Y. Li were supported by the University of Houston's internal funds and the Sloan Foundation via the Houston Advanced Research Center (contract no. UH0421). H.-Y. Li and L. R. Leung were also supported by the U.S. Department of Energy Office of Science Biological and Environmental Research as part of the Earth System Model Development program area through the collaborative, multi-program Integrated Coastal Modeling (ICoM) project.

References

Akiba, T., Sano, S., Yanase, T., Ohta, T., & Koyama, M. (2019). Optuna: A next-generation hyperparameter optimization framework. *Proceedings of the 25th ACM SIGKDD International Conference on Knowledge Discovery & Data Mining*, 2623–2631. https://doi.org/10.48550/arXiv.1907.10902

American Society of Civil Engineers. (1996). *Hydrology handbook*. Author. https://doi.org/10.1061/9780784401385

Argue, J. R., & Pezzaniti, D. (2012). Use of WSUD ‘ source control ’ practices to manage floodwaters in urbanising landscapes: Developed and ultra-developed catchments. In *Proceedings of STORMWATER 2012, national conference of the stormwater industry*. Retrieved from https://api.semanticscholar.org/CorpusID:202609239

Avellaneda, P. M., Jefferson, A. J., Grieser, J. M., & Bush, S. A. (2017). Simulation of the cumulative hydrological response to green infrastructure. *Water Resources Research*, *53*(4), 3087–3101. https://doi.org/10.1002/2016wr019836

Blondel, V. D., Guillaume, J.-L., Lambiotte, R., & Lefebvre, E. (2008). Fast unfolding of communities in large networks. *Journal of Statistical Mechanics: Theory and Experiment*, *2008*(10), P10008. https://doi.org/10.1088/1742-5468/2008/10/P10008

Brater, E. F. (1968). Steps toward a better understanding of urban runoff processes. *Water Resources Research*, *4*(2), 335–347. https://doi.org/10.1029/WR004i002p00335

Brown, S., Schall, J., Morris, J., Doherty, C., Stein, S., & Warner, J. (2009). *Urban drainage design manual: Hydraulic engineering circular 22* (3ed edn.). Federal National Highway Institute. Retrieved from https://www.fhwa.dot.gov/engineering/hydraulics/pubs/10009/10009.pdf

Burns, M. J., Schubert, J. E., Fletcher, T. D., & Sanders, B. F. (2015). Testing the impact of at-source stormwater management on urban flooding through a coupling of network and overland flow models. *WIREs Water*, *2*(4), 291–300. https://doi.org/10.1002/wat2.1078

Chegini, T., & Li, H.-Y. (2022). An algorithm for deriving the topology of belowground urban stormwater networks. *Hydrology and Earth System Sciences*, *26*(16), 4279–4300. https://doi.org/10.5194/hess-26-4279-2022

Chegini, T., Li, H.-Y., & Leung, L. (2021). HyRiver: Hydroclimate data retriever. *Journal of Open Source Software*, *6*(66), 3175. https://doi.org/10.21105/joss.03175

Chegini, T., Li, H.-Y., Yang, Y. C. E., Blöschl, G., & Leung, R. (2024). A scalable urban hydrologic framework: Incorporating network-level storm drainage pipes representation [Software]. *Zenodo*. https://doi.org/10.5281/zenodo.13351050

Chen, M., Nabih, S., Brauer, N. S., Gao, S., Gourley, J. J., Hong, Z., et al. (2020). Can remote sensing technologies capture the extreme precipitation event and its cascading hydrological response? A case study of hurricane harvey using EF5 modeling framework. *Remote Sensing*, *12*(3), 445. https://doi.org/10.3390/rs12030445

Chen, W., Wu, H., Kimball, J. S., Alfieri, L., Nanding, N., Li, X., et al. (2022). A coupled river basin-urban hydrological model (DRIVE-Urban) for real-time urban flood modeling. *Water Resources Research*, *58*(11), e2021WR031709. https://doi.org/10.1029/2021WR031709

Chocat, B., Krebs, P., Marsalek, J., Rauch, W., & Schilling, W. (2001). Urban drainage redefined: From stormwater removal to integrated management. *Water Science and Technology*, *43*(5), 61–68. https://doi.org/10.2166/wst.2001.0251

Chow, V. T. (1959). *Open-channel hydraulics*. McGraw-Hill.

Chow, V. T., Maidment, D. R., & Mays, L. W. (1988). Applied hydrology.

Cosgrove, B., Gochis, D., Flowers, T., Dugger, A., Ogden, F., Graziano, T., et al. (2024). NOAA’S national water model: Advancing operational hydrology through continental-scale modeling. *JAWRA Journal of the American Water Resources Association*, *60*(2), 247–272. https://doi.org/10.1111/1752-1688.13184

Cristiano, E., ten Veldhuis, M.-c., & Van De Giesen, N. (2017). Spatial and temporal variability of rainfall and their effects on hydrological response in urban areas–a review. *Hydrology and Earth System Sciences*, *21*(7), 3859–3878. https://doi.org/10.5194/hess-21-3859-2017

Cunge, J. A., & Wegner, M. (1964). Intégration numérique des équations d’écoulement de barré de Saint-Venant par un schéma implicite de différences finies. *La Houille Blanche*, *50*(1), 33–39. https://doi.org/10.1051/lhb/1964002

Decharme, B., Delire, C., Minvielle, M., Colin, J., Vergnes, J.-P., Alias, A., et al. (2019). Recent changes in the ISBA-CTRIP land surface system for use in the CNRM-CM6 climate model and in global off-line hydrological applications. *Journal of Advances in Modeling Earth Systems*, *11*(5), 1207–1252. https://doi.org/10.1029/2018MS001545

Dewitz, J. (2021). National Land Cover Database (NLCD) 2019 products. *U.S. Geological Survey*. https://doi.org/10.5066/P9KZCM54

DHI. (2023). Mike urban: Integrated urban water modelling [Computer software manual]. https://www.mikepoweredbydhi.com/products/mike-urbanforthelatestversion

Dong, B., Xia, J., Zhou, M., Li, Q., Ahmadian, R., & Falconer, R. A. (2022). Integrated modeling of 2D urban surface and 1D sewer hydrodynamic processes and flood risk assessment of people and vehicles. *Science of the Total Environment*, *827*, 154098. https://doi.org/10.1016/j.scitotenv.2022.154098

Durran, D. R. (2010). Ordinary differential equations. In D. R. Durran (Ed.), *Numerical methods for fluid dynamics: With applications to geophysics* (pp. 35–87). Springer. https://doi.org/10.1007/978-1-4419-6412-0_2

E3SM Project. (2024). Energy Exascale Earth System Model v3.0.0 [Computer Software]. https://doi.org/10.11578/E3SM/dc.20240301.3

EPA. (2018). Compendium of clear, specific and measurable permitting examples. https://www.epa.gov/sites/default/files/2018-11/documents/final_compendium_intro_document_rev-11-15-18.pdf

Fall, G., Kitzmiller, D., Pavlovic, S., Zhang, Z., Patrick, N., St. Laurent, M., et al. (2023). The office of water prediction’s analysis of record for calibration, version 1.1: Dataset description and precipitation evaluation. *JAWRA Journal of the American Water Resources Association*, *59*(6), 1246–1272. https://doi.org/10.1111/1752-1688.13143

Fortunato, S., & Castellano, C. (2007). Community structure in graphs. https://doi.org/10.48550/arXiv.0712.2716

Fraga, I., Cea, L., Puertas, J., Suárez, J., Jiménez, V., & Jácome, A. (2016). Global sensitivity and GLUE-based uncertainty analysis of a 2D-1D Dual Urban Drainage Model. *Journal of Hydrologic Engineering*, *21*(5), 04016004. https://doi.org/10.1061/(ASCE)HE.1943-5584.0001335

Freni, G., Mannina, G., & Viviani, G. (2009). Uncertainty in urban stormwater quality modelling: The influence of likelihood measure formulation in the GLUE methodology. *Science of the Total Environment*, *408*(1), 138–145. https://doi.org/10.1016/j.scitotenv.2009.09.029

Garschagen, M., & Romero-Lankao, P. (2015). Exploring the relationships between urbanization trends and climate change vulnerability. *Climatic Change*, *133*(1), 37–52. https://doi.org/10.1007/s10584-013-0812-6

Grimm, N. B., Faeth, S. H., Golubiewski, N. E., Redman, C. L., Wu, J., Bai, X., & Briggs, J. M. (2008). Global change and the ecology of cities. *Science*, *319*(5864), 756–760. https://doi.org/10.1126/science.1150195

Guo, K., Guan, M., & Yu, D. (2021). Urban surface water flood modelling – A comprehensive review of current models and future challenges. *Hydrology and Earth System Sciences*, *25*(5), 2843–2860. https://doi.org/10.5194/hess-25-2843-2021

Gupta, H. V., Kling, H., Yilmaz, K. K., & Martinez, G. F. (2009). Decomposition of the mean squared error and NSE performance criteria: Implications for improving hydrological modelling. *Journal of Hydrology*, *377*(1), 80–91. https://doi.org/10.1016/j.jhydrol.2009.08.003

Harrigan, S., Zsoter, E., Alfieri, L., Prudhomme, C., Salamon, P., Wetterhall, F., et al. (2020). Glofas-era5 operational global river discharge reanalysis 1979–present. *Earth System Science Data*, *12*(3), 2043–2060. https://doi.org/10.5194/essd-12-2043-2020

Heilman, J. (2022). Hydraulics manual. Design office, engineering and regional operations division. https://wsdot.wa.gov/engineering-standards/all-manuals-and-standards/manuals/hydraulics-manual

Hicks, W. (1944). *A method of computing urban runoff*. Transactions of the American Society of Civil Engineers.

Hung, F., Harman, C. J., Hobbs, B. F., & Sivapalan, M. (2020). Assessment of climate, sizing, and location controls on green infrastructure efficacy: A timescale framework. *Water Resources Research*, *56*(5), e2019WR026141. https://doi.org/10.1029/2019WR026141

Hutchins, M. G., McGrane, S. J., Miller, J. D., Hagen-Zanker, A., Kjeldsen, T. R., Dadson, S. J., & Rowland, C. S. (2017). Integrated modeling in urban hydrology: Reviewing the role of monitoring technology in overcoming the issue of 'big data'requirements. *Wiley Interdisciplinary Reviews: Water*, *4*(1), e1177. https://doi.org/10.1002/wat2.1177

Iwanaga, T., Usher, W., & Herman, J. (2022). Toward SALib 2.0: Advancing the accessibility and interpretability of global sensitivity analyses. *Socio-Environmental Systems Modelling*, *4*, 18155. https://doi.org/10.18174/sesmo.18155

Jenks, G. (1977). *Optimal data classification for choropleth maps*. University of Kansas.

King, D. M., & Perera, B. J. C. (2013). Morris method of sensitivity analysis applied to assess the importance of input variables on urban water supply yield – A case study. *Journal of Hydrology*, *477*, 17–32. https://doi.org/10.1016/j.jhydrol.2012.10.017

Knoben, W. J. M., Freer, J. E., & Woods, R. A. (2019). Technical note: Inherent benchmark or not? Comparing Nash–Sutcliffe and Kling–Gupta efficiency scores. *Hydrology and Earth System Sciences*, *23*(10), 4323–4331. https://doi.org/10.5194/hess-23-4323-2019

Krajewski, A., Sikorska-Senoner, A. E., Hejduk, A., & Hejduk, L. (2020). Variability of the initial abstraction ratio in an urban and an agroforested catchment. *Water*, *12*(2), 415. https://doi.org/10.3390/w12020415

Lam, S. K., Pitrou, A., & Seibert, S. (2015). Numba: A llvm-based python jit compiler. In *Proceedings of the second workshop on the llvm compiler infrastructure in hpc* (pp. 1–6).

Li, H., & Sivapalan, M. (2011). Effect of spatial heterogeneity of runoff generation mechanisms on the scaling behavior of event runoff responses in a natural river basin. *Water Resources Research*, *47*(3). https://doi.org/10.1029/2010wr009712

Li, H., Wigmosta, M. S., Wu, H., Huang, M., Ke, Y., Coleman, A. M., & Leung, L. R. (2013). A physically based runoff routing model for land surface and earth system models. *Journal of Hydrometeorology*, *14*(3), 808–828. https://doi.org/10.1175/JHM-D-12-015.1

Liu, Z., Merwade, V., & Jafarzadegan, K. (2019). Investigating the role of model structure and surface roughness in generating flood inundation extents using one- and two-dimensional hydraulic models. *Journal of Flood Risk Management*, *12*(1), e12347. https://doi.org/10.1111/jfr3.12347

McGrath, G., Kaeseberg, T., Reyes-Silva, J. D., Jawitz, J. W., Blumensaat, F., Borchardt, D., et al. (2019). Network topology and rainfall controls on the variability of combined sewer overflows and loads. *Water Resources Research*, *55*(11), 9578–9591. https://doi.org/10.1029/2019wr025336

Meyers, S. D., Landry, S., Beck, M. W., & Luther, M. E. (2021). Using logistic regression to model the risk of sewer overflows triggered by compound flooding with application to sea level rise. *Urban Climate*, *35*, 100752. https://doi.org/10.1016/j.uclim.2020.100752

Miller, J. D., & Hutchins, M. (2017). The impacts of urbanisation and climate change on urban flooding and urban water quality: A review of the evidence concerning the United Kingdom. *Journal of Hydrology: Regional Studies*, *12*, 345–362. https://doi.org/10.1016/j.ejrh.2017.06.006

Mishra, S. K., Pandey, A., & Singh, V. P. (2012). Special issue on Soil Conservation Service Curve Number (SCS-CN) Methodology. *Journal of Hydrologic Engineering*, *17*(11), 1157. https://doi.org/10.1061/(ASCE)HE.1943-5584.0000694

Moore, R., & Clarke, R. (1981). A distribution function approach to rainfall runoff modeling. *Water Resources Research*, *17*(5), 1367–1382. https://doi.org/10.1029/wr017i005p01367

Morales, V. M., Quijano, J. C., Schmidt, A., & Garcia, M. H. (2016). Innovative framework to simulate the fate and transport of nonconservative constituents in urban combined sewer catchments. *Water Resources Research*, *52*(11), 9164–9181. https://doi.org/10.1002/2016wr018807

Nanía, L. S., León, A. S., & García, M. H. (2015). Hydrologic-Hydraulic Model for simulating dual drainage and flooding in urban areas: Application to a catchment in the metropolitan area of Chicago. *Journal of Hydrologic Engineering*, *20*(5), 04014071. https://doi.org/10.1061/(ASCE)HE.1943-5584.0001080

Nash, J. E. (1957). *The form of the instantaneous unit hydrograph.[W:] surface water, prevision, evaporation. International association of sciences and hydrological publications* (Vol. 45). IAHS Press.

National Oceanic and Atmospheric Administration. (2024). NOAA national water model conus retrospective dataset. Retrieved from https://registry.opendata.aws/nwm-archive

Naves, J., Anta, J., Puertas, J., Regueiro-Picallo, M., & Suárez, J. (2019). Using a 2D Shallow Water Model to assess Large-Scale Particle Image Velocimetry (LSPIV) and Structure from Motion (SfM) techniques in a street-scale urban drainage physical model. *Journal of Hydrology*, *575*, 54–65. https://doi.org/10.1016/j.jhydrol.2019.05.003

Officials, N. A. o. C. T. (2017). *Urban street stormwater guide*. Island Press.

Rossman, L., & Simon, M. (2022). *Addendum to the storm water management model reference manual volume Ii - hydraulics*. U.S. Environmental Protection Agency.

Ruano, M., Ribes, J., Seco, A., & Ferrer, J. (2012). An improved sampling strategy based on trajectory design for application of the Morris method to systems with many input factors. *Environmental Modelling and Software*, *37*, 103–109. https://doi.org/10.1016/j.envsoft.2012.03.008

Salvadore, E., Bronders, J., & Batelaan, O. (2015). Hydrological modelling of urbanized catchments: A review and future directions. *Journal of Hydrology*, *529*, 62–81. https://doi.org/10.1016/j.jhydrol.2015.06.028

Schwarz, G. E., Jackson, S. E., & Wieczorek, M. E. (2018). *Select attributes for NHDPlus version 2.1 reach catchments and modified network routed upstream watersheds for the conterminous United States*. U.S. Geological Survey. https://doi.org/10.5066/F7765D7V

SCS. (1972). Hydrology. In *National engineering handbook* (p. 762). US Department of Agriculture.

Shrestha, S., Cui, S., Xu, L., Wang, L., Manandhar, B., & Ding, S. (2021). Impact of land use change due to urbanisation on surface runoff using GIS-based SCS–CN method: A case study of Xiamen City, China. *Land*, *10*(8), 839. https://doi.org/10.3390/land10080839

Song, X., Zhang, J., Zhan, C., Xuan, Y., Ye, M., & Xu, C. (2015). Global sensitivity analysis in hydrological modeling: Review of concepts, methods, theoretical framework, and applications. *Journal of Hydrology*, *523*, 739–757. https://doi.org/10.1016/j.jhydrol.2015.02.013

Staudt, C. L., & Meyerhenke, H. (2016). Engineering parallel algorithms for community detection in massive networks. *IEEE Transactions on Parallel and Distributed Systems*, *27*(1), 171–184. https://doi.org/10.1109/TPDS.2015.2390633

Staudt, C. L., Sazonovs, A., & Meyerhenke, H. (2015). NetworKit: A tool suite for large-scale complex network analysis (No. arXiv:1403.3005). *arXiv*. https://doi.org/10.48550/arXiv.1403.3005

Sytsma, A., Crompton, O., Panos, C., Thompson, S., & Kondolf, G. M. (2022). Quantifying the uncertainty created by non-transferable model calibrations across climate and land cover scenarios: A case study with SWMM. *Water Resources Research*, *58*(2). https://doi.org/10.1029/2021wr031603

TCEQ. (2023). Texas wastewater outfalls. Retrieved from https://tceq.maps.arcgis.com/apps/webappviewer/index.html?id=d47b9419f42c49dea592203aeda99da1

Tholin, A. L., & Keifer, C. J. (1959). The hydrology of urban runoff. *Journal of the Sanitary Engineering Division*, *85*(2), 47–106. https://doi.org/10.1061/JSEDAI.0000218

Tian, F., Li, H., & Sivapalan, M. (2012). Model diagnostic analysis of seasonal switching of runoff generation mechanisms in the blue River Basin, Oklahoma. *Journal of Hydrology*, *418–419*, 136–149. https://doi.org/10.1016/j.jhydrol.2010.03.011

TxDOT. (2019). Hydraulic design manual of Texas department of transportation. Retrieved from http://onlinemanuals.txdot.gov/txdotmanuals/hyd/index.htm

UDFC. (2016). Urban storm drainage criteria manual: Volume 1, management, hydrology, and hydraulics. *Urban Drainage and Flood Control District*.

USACE. (2022). HEC-HMS user's manual. Retrieved from https://www.hec.usace.army.mil/confluence/hmsdocs/hmsum/latest

U.S. Geological Survey. (2019). National hydrography dataset. Retrieved from https://www.usgs.gov/national-hydrography/access-national-hydrography-products

U.S. Geological Survey. (2022). USGS 3D Elevation Program Digital Elevation Model. Retrieved from https://elevation.nationalmap.gov/arcgis/rest/services/3DEPElevation/ImageServer

van Oldenborgh, G. J., van der Wiel, K., Sebastian, A., Singh, R., Arrighi, J., Otto, F., et al. (2017). Attribution of extreme rainfall from hurricane Harvey, August 2017. *Environmental Research Letters*, *12*(12), 124009. https://doi.org/10.1088/1748-9326/aa9ef2

Vemula, S., Raju, K. S., Veena, S. S., & Kumar, A. S. (2018). Urban floods in Hyderabad, India, under present and future rainfall scenarios: A case study. *Natural Hazards*, *95*(3), 637–655. https://doi.org/10.1007/s11069-018-3511-9

Wang, D. (2018). A new probability density function for spatial distribution of soil water storage capacity leads to the SCS curve number method. *Hydrology and Earth System Sciences*, *22*(12), 6567–6578. https://doi.org/10.5194/hess-22-6567-2018

Watanabe, S. (2023). Tree-structured parzen estimator: Understanding its algorithm components and their roles for better empirical performance. https://doi.org/10.48550/arXiv.2304.11127

Wong, B. P., & Kerkez, B. (2018). Real-time control of urban headwater catchments through linear feedback: Performance, analysis, and site selection. *Water Resources Research*, *54*(10), 7309–7330. https://doi.org/10.1029/2018wr022657

Wu, H., Adler, R. F., Tian, Y., Huffman, G. J., Li, H., & Wang, J. (2014). Real-time global flood estimation using satellite-based precipitation and a coupled land surface and routing model. *Water Resources Research*, *50*(3), 2693–2717. https://doi.org/10.1002/2013wr014710

Wu, S., Tetzlaff, D., Yang, X., & Soulsby, C. (2022). Identifying dominant processes in time and space: Time-varying spatial sensitivity analysis for a Grid-Based Nitrate Model. *Water Resources Research*, *58*(8), e2021WR031149. https://doi.org/10.1029/2021WR031149

Xia, Y., Mitchell, K., Ek, M., Sheffield, J., Cosgrove, B., Wood, E., et al. (2012). Continental-scale water and energy flux analysis and validation for the North American land data assimilation system project phase 2 (NLDAS-2): 1. Intercomparison and application of model products. *Journal of Geophysical Research*, *117*(D3). https://doi.org/10.1029/2011JD016048

Yang, L., Smith, J. A., Wright, D. B., Baeck, M. L., Villarini, G., Tian, F., & Hu, H. (2013). Urbanization and climate change: An examination of nonstationarities in urban flooding. *Journal of Hydrometeorology*, *14*(6), 1791–1809. https://doi.org/10.1175/jhm-d-12-095.1

Yao, L., Libera, D. A., Kheimi, M., Sankarasubramanian, A., & Wang, D. (2020a). The roles of climate forcing and its variability on streamflow at daily, monthly, annual, and long-term scales. *Water Resources Research*, *56*(7). https://doi.org/10.1029/2020WR027111

Yao, L., Libera, D. A., Kheimi, M., Sankarasubramanian, A., & Wang, D. (2020b). The roles of climate variability on runoff at daily, monthly, annual, and long-term scales. *Water Resources Research*, *22*(12), 6567–6578. https://doi.org/10.5194/hess-22-6567-2018